Molecular Microbiology (2008) 68(4), 997–1017 ■
doi:10.1111/j.1365-2958.2008.06199.x
First published online 8 April 2008

A novel autotransporter of uropathogenic *Proteus mirabilis* is both a cytotoxin and an agglutinin

Praveen Alamuri and Harry L. T. Mobley*
Department of Microbiology and Immunology, University of Michigan Medical School, Ann Arbor, MI 48109-0620, USA.

Summary

One of the six predicted *Proteus mirabilis* autotransporters (ATs), ORF c2341, is predicted to contain a serine protease motif and was earlier identified as an immunogenic outer membrane protein in *P. mirabilis*. The 3.2 kb gene encodes a 117 kDa protein with a 58-amino-acid-long signal peptide, a 75-kDa-long N-terminal passenger domain and a 30-kDa-long C-terminal translocator. Affinity-purified 110 kDa AT exhibited chymotrypsin-like activity and hydrolysed *N*-Suc–Ala–Ala–Pro–Phe–*p*Na and *N*-Suc–Ala–Ala–Pro–Leu–*p*Na with a K_M of 22 μM and 31 μM, respectively, under optimal pH of 8.5–9.0 in a Ca^{2+}-dependent manner. Activity was inhibited by subtilase-specific inhibitors leupeptin and chymostatin. Both the cell-associated and purified form elicited cytopathic effects on cultured kidney and bladder epithelial cells. Substrate hydrolysis as well as cytotoxicity was associated with the passenger domain and was compromised upon mutation of any of the catalytic residues (Ser366, His147 and Asp533). At alkaline pH and optimal cell density, the AT also promoted autoaggregation of *P. mirabilis* and this function was independent of its protease activity. Cytotoxicity, autoaggregation and virulence were significantly reduced in an isogenic *pta* mutant of *P. mirabilis*. *Proteus* toxic agglutinin (Pta) represents a novel autotransported cytotoxin with no bacterial homologues that works optimally in the alkalinized urinary tract, a characteristic of urease-mediated urea hydrolysis during *P. mirabilis* infection.

Introduction

Protein secretion in Gram-negative bacteria facilitates nutrient acquisition, initiates interactions with the eukaryotic host and mediates bacterial cell–cell communication. For pathogenic bacteria, protein secretion by type II, III and IV systems is often required for full virulence. These protein secretion systems may export toxic proteins across the outer membrane (OM) or inject them directly into the host cell (Stathopoulos *et al.*, 2000; Cianciotto, 2005; Mota and Cornelis, 2005; Backert and Meyer, 2006). In the last two decades, a new family of virulence proteins that are unique to Gram-negative bacterial pathogens, known as autotransporters (ATs), was discovered. These proteins are exported to the outside of the cell by the type V or the AT secretion pathway. ATs are modular proteins with three domains: a long leader peptide required for Sec-dependent transport across the inner membrane, an N-terminal passenger or alpha domain that determines the virulence function of the AT, and a C-terminal hydrophobic translocator or beta domain that facilitates the translocation of the alpha domain across the OM into the extracellular milieu (Henderson *et al.*, 1998). This basic structural organization of ATs is highly conserved, but their functions vary widely; this diversity is typically attributed to the activity of the surface-expressed alpha or passenger moiety. The passenger domain may mediate host invasion, autoagglutination or haemagglutination, confer resistance against host serum proteins and antibodies, or act as a secreted cytotoxin (Henderson and Nataro, 2001). Due to their surface localization or release from the bacterium, ATs directly interact with the host and hence have been instrumental in elucidating previously unknown molecular events during host–pathogen interactions. In two examples, purified ATs Hap from *Haemophilus influenzae* (Liu *et al.*, 2004) and BrkA from *Bordetella pertussis* (Cainelli Gebara *et al.*, 2007) were used as vaccines against these pathogens and more ATs are being pursued as potential surface-expressed antigens (Wells *et al.*, 2007).

Proteus mirabilis, a Gram-negative dimorphic human uropathogen differentiates between a vegetative swimmer and a hyper-flagellated swarmer cell. *P. mirabilis* causes complicated urinary tract infections (UTIs) among individuals with anatomical abnormalities of the urinary tract or in patients with long-term indwelling catheters and may cause bacteraemia among the elderly (Mobley, 1996a), making it one of the most common nosocomial infections.

Accepted 3 March, 2008. *For correspondence. E-mail hmobley@umich.edu; Tel. (+1) 734 764 1466; Fax (+1) 734 763 7163.

Fig. 1. Pta domains, active site and purification.
A. Schematic representation of the structure of Pta. The 1072-amino-acid-long autotransporter protein (upper construct) with a signal sequence (grey shade), N-terminal passenger domain (spotted) and the C-terminal translocator domain (white) with the positions of antiparallel beta sheets (black bars) shown. The protein is annotated as a subtilisin-like alkaline serine protease. The amino acids Ser366, His146 and Asp533 that form the putative catalytic serine protease triad are indicated in the passenger domain. Schematic representation of the expression constructs is shown (lower construct). In each case Pta was cloned into pET21A to express it as a C-terminal 6X-His tag fusion protein.
B. Alignment of the active site of Pta and its homologues. Alignment of putative catalytic domains of Pta with the sequence of Ser, His and Asp. Pta, *Proteus* toxic agglutinin of *P. mirabilis*; SubA, Toxic subunit of AB5 type toxin SubAB of STEC; Fls, Fervidolysin of *Fervidobacterium pennivorans*; and PspA, Serine protease A of *Pseudomonas chlororaphis*. The numbers above the Pta fragments indicate the residue number of the terminal amino acids in Pta. Alternative consensus residues at a given position are shown vertically. The known active-site residues in each subtilase catalytic domain are shown in bold type. The asterisk indicates Pta residues that do not match the consensus sequence.
C. Expression and purification of Pta and $Pta_{(S366A)}$. Whole-cell or outer membrane protein (6 μg) of *E. coli* BL21plysS expressing vector control (CTL), Pta or $Pta_{(S366A)}$ (Pta*) was separated on a 10% SDS-PAGE. The two arrows (at 100 kDa marker) indicate the larger pre-protein and the smaller mature Pta protein. The arrow at ~30 kDa indicates OmpA used as a marker for enriched OM protein fraction. U = uninduced culture; I = *E. coli* BL21plysS induced with 1 mM IPTG; and M = molecular size marker. The next to last lane represents the affinity-purified ~110 kDa mature form of Pta to ~95% homogeneity. Mobility of protein standards is shown in kDa.

The genome sequence of the catheter-associated *P. mirabilis* strain HI4320 reveals 3685 open reading frames in a 4.3 Mb single circular chromosome along with a stable 36 kb plasmid (Pearson *et al.*, 2008). Six putative ATs are annotated: three (Orfs c0844, 2126 and c2341) as proteases and three (Orfs 2122, 2174 and 2575) as putative adhesins or haemagglutinin-like ATs (Pearson *et al.*, 2008). Putative AT c2341 has been recognized in our laboratory as a surface-expressed antigenic protein when stained with antisera from mice chronically infected with *P. mirabilis*, suggesting a role for this protein *in vivo* (G.R. Nielubowicz and H.L.T. Mobley, unpubl. data). It is annotated as an AT with a subtilisin-like serine protease motif. Subtilisins are pre-protein convertases that are known to catalyse key functions in the cell such as protein activation as a post-translational modification, and cellular trafficking making them significant therapeutic targets in both eukaryotic and prokaryotic systems (Hutton, 1990). Together these features identify c2341 as a candidate virulence factor of *P. mirabilis*.

In this study we characterized the structure and function of c2341 and, using a mouse model of ascending UTI, established its significance in the pathogenesis of *P. mirabilis* UTIs. The protein was purified to homogeneity, and the biochemical characteristics of the putative protease were determined using synthetic substrates and enzyme inhibitors. The nature of its interaction with human bladder and kidney epithelial cell lines was elucidated using *in vitro* cell culture studies. Unique characteristics of this AT indicate that it functions both as a bacterial cell–cell agglutinin and as an OM-associated cytotoxic protease with an alkaline pH optimum. Therefore, we designated this novel autotransported cytotoxin Pta, for *Proteus* toxic agglutinin.

Results

Structure of Pta

The *pta* gene (c2341) of *P. mirabilis* strain HI4320 is annotated as an AT with a subtilisin-like protease motif. The 3183-bp-long gene encodes a hypothetical 1072-amino-acid-long protein with a theoretical molecular size of 117 kDa. Using BLAST analysis, no proteins shared significant amino acid sequence identity with the putative passenger domain of Pta. The closest homologues, displaying only ~20% amino acid sequence identity, were the thermostable enzyme Fervidolysin (Fls) from *Fervidobacterium pennivorans* (Kluskens *et al.*, 2002), Serine protease A (PspA), a protease-like putative AT from *Pseudomonas chlororaphis* (Swiss-Prot/Tr-EMBL), and SubA subunit of SubAB toxin from Shiga-Toxin producing *Escherichia coli* (Paton *et al.*, 2004). Amino acid sequence identity within the alpha domain was restricted to regions spanning the identified catalytic residues of these proteases (Fig. 1B). Using the N-terminus sequencing, the signal sequence was identified to be 40 amino acids long with the potential cleavage site between residues A^{40} and Y^{41}. The amino acid sequence of c234l analysed using MOTIF search found that the amino acids 1–730 form the passenger or the alpha domain of the putative AT. The protein belongs to the family of serine proteases with Ser366, His147 and Asp533 forming the putative serine catalytic triad of the protease (Fig. 1A and B). No RGD motifs or lipid attachment motifs were detected in the passenger domain suggesting that the protein does not bind to any known receptors on the eukaryotic host.

C-terminal residues 731–1072 were predicted to constitute the beta domain of the AT. The C-terminus shows similarity with various OM proteins and beta domains of ATs from *Pseudomonas* spp. (data not shown). Analysis of the probable membrane topology of this protein revealed that hydrophobic amino acids account for more than 50% of this domain with at least nine different stretches of hydrophobic residues with intermittent hydrophilic residues, which together form the antiparallel beta sheets and the connecting loops of the OM beta barrel of the translocator (Fig. 1A). The sequence terminated in the YIFQYNS motif, which partially conforms to the typical AT

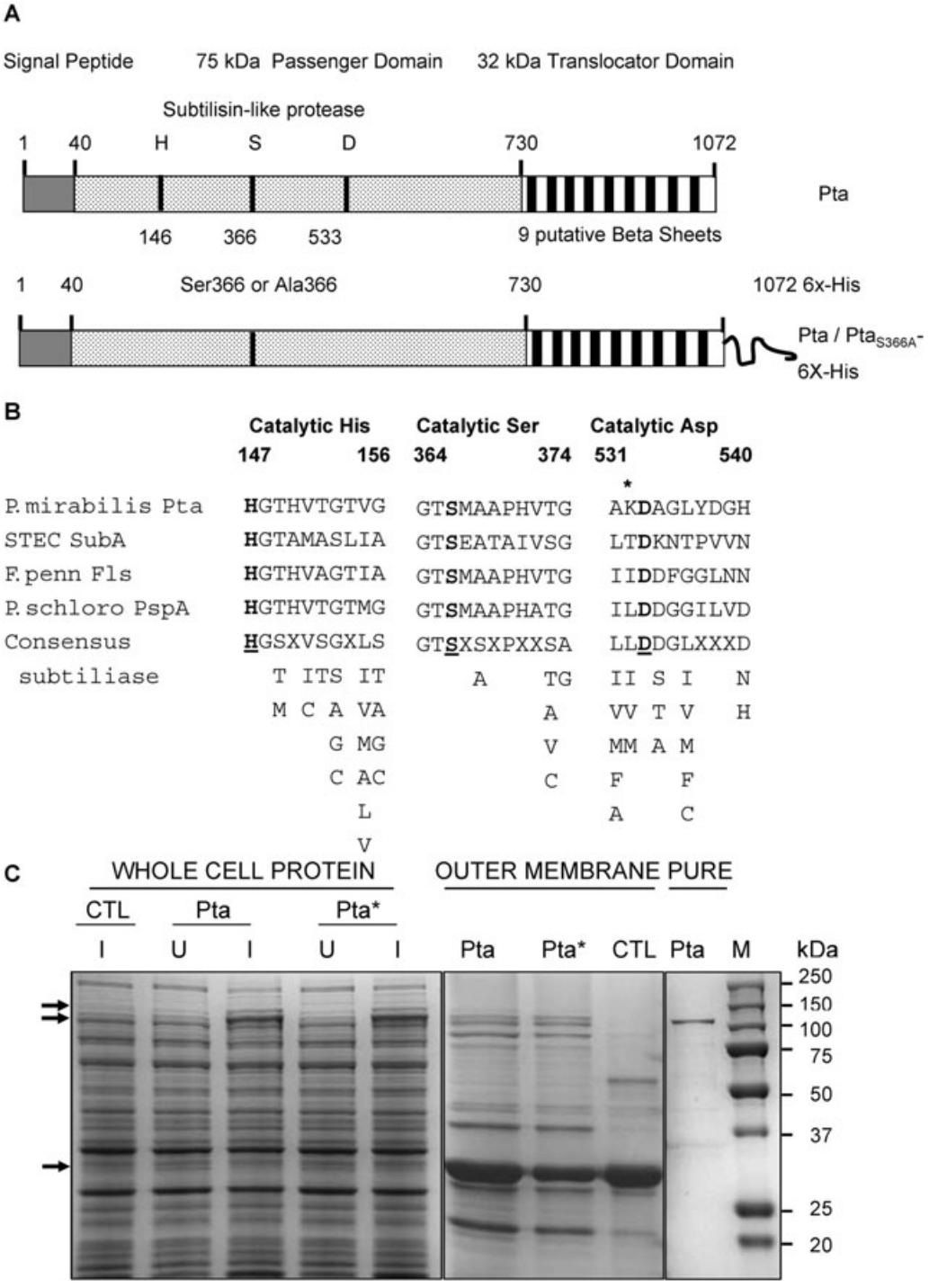

motif (Y/V/I/F/W)-X-(F/Y/W). Interestingly, Pta is cysteine-deficient, in accordance with an observation that known AT proteins contain no or few cysteine (Henderson *et al.*, 2004).

Expression and purification of Pta and Pta-α

Pta wild type, active-site serine mutant Ser366Ala denoted as Pta* or the Ser366Ala and His147Ala double mutant were overexpressed as recombinant proteins in *E. coli* BL21plysS. Pta was purified as a ~110 kDa protein in either case from the OM of the bacterium (Fig. 1C). Two important features of Pta were observed from the above results; first, Pta exists as two forms, a larger ~120 kDa protein and a shorter protein of ~110 kDa, and the latter species is the major form. Interestingly, the S366A or S366A/H147A active-site mutants showed a similar effi-

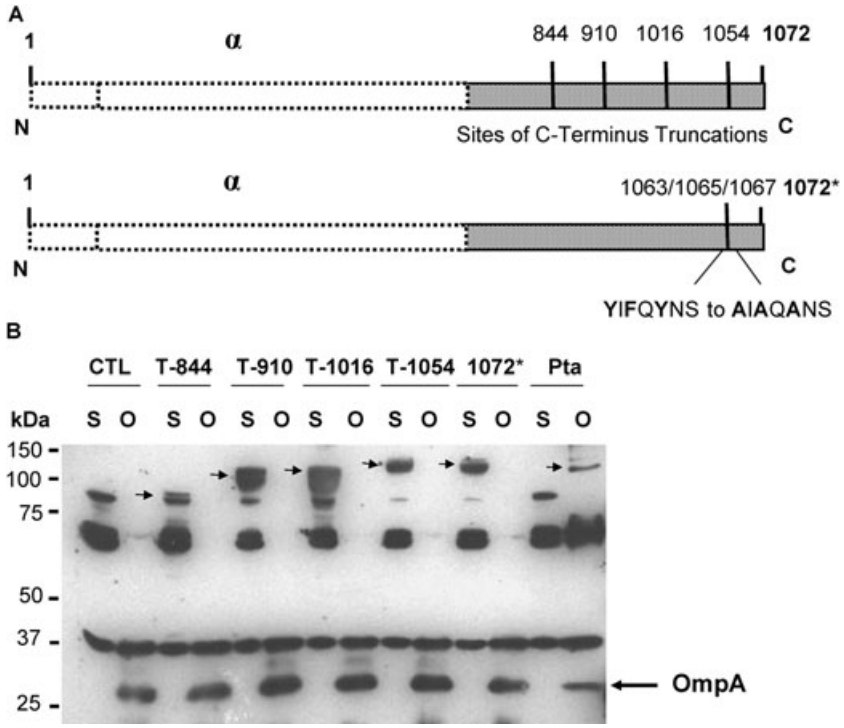

Fig. 2. Role of beta domain in Pta localization.
A. Schematic representation of amino acid positions at which truncations (T) were made in the beta domain of Pta (top). Pta-1072* with amino acid residues Tyr1063, Phe1065 and Tyr1067 altered to respective Ala is shown (bottom).
B. Each of the truncated or altered versions was expressed in *E. coli* BL21plysS and 6 μg each of the soluble (S) or the outer membrane (O) protein fractions was electrophoresed on a 10% SDS-PAGE. *E. coli* BL21plysS carrying pET21A as control (CTL). Proteins were immunoblotted with Anti-Pta antiserum (1:750) and Goat Anti-Rabbit IgG-HRP conjugate (1:20000). Arrows identify the truncated Pta.

ciency in processing, implying no role for Ser366 in this process. We confirmed the identity of both proteins as Pta by mass spectrometric analysis. In addition, N-terminal sequencing of the ~110 kDa protein band was determined to be EKGQVFDVDG, which aligns well with the amino acid sequence of Pta between residues Glu127 and Gly136. This confirms that the 120 kDa protease undergoes a secondary processing between residues Y^{126} and E^{127} to yield a catalytically mature 110 kDa form, a feature commonly seen in eukaryotic subtilisin-like proteases (Steiner, 1998). The OM fraction of the Pta-expressing *E. coli* BL21plysS also shows a protein with a molecular weight of ~20 kDa (Fig. 1C). The protein band was identified by mass spectrometry as a cleaved product of an unrelated protein PhoA, an alkaline phosphatase precursor in *E. coli*.

Second, the mature Pta is stably expressed as a 110 kDa protein in the OM suggesting that the passenger domain of Pta is not cleaved away from the translocator as seen in most protease-like ATs; rather it remains intact in the OM (Fig. 1C). We confirmed this observation by comparing the protein profiles of culture supernatants from *E. coli* BL21 expressing the pET21A vector control, or that expressing each of the Pta variants, but found no indication of alpha/passenger domain processing at the OM (data not shown). As this phenomenon (of intact alpha and beta domains) is seen with ATs that are adhesins, haemagglutinins or agglutinins, we hypothesized a similar role for Pta in *P. mirabilis*.

Significance of the beta domain in OM localization of Pta

Autotransporter proteins that mediate the functions of cell–cell agglutination or adhesion to the host (as hypothesized for Pta) show varied lengths of the beta domain. ATs with as short as 60- to 100-amino-acid-long beta domains are seen in case of YadA (*Yersinia enterocolitica*), Hia and Hsf (*H. influenzae*) or NadA (*Neisseria meningitidis*) that assume trimeric forms for the successful translocation of the passenger domains across the OM and form a functional adhesive pocket on the surface of the pathogen (Cotter *et al.*, 2005; 2006). To determine whether the entire translocator domain of the Pta is required for the translocation of Pta-α across the OM, we made eight different truncations in the beta domain of Pta at positions corresponding to the predicted hydrophilic helices that bridge two adjacent hydrophobic beta sheets in the translocator. We also generated multiple point mutations (Y1063A, F1065A and Y1067A) towards the C-terminus of the beta domain to determine the significance of the hydrophobic residues in the translocation of Pta into the OM of the cell. Figure 2A shows the schematic of four of these truncations (T-844, T-910, T-1016 and T-1054) and the altered Pta (designated as 1072*). Each of these versions was individually expressed in *E. coli* BL21plysS, and protein localization was determined by immunostaining with Anti-Pta antiserum (Fig. 2B). All truncated versions were stably expressed in

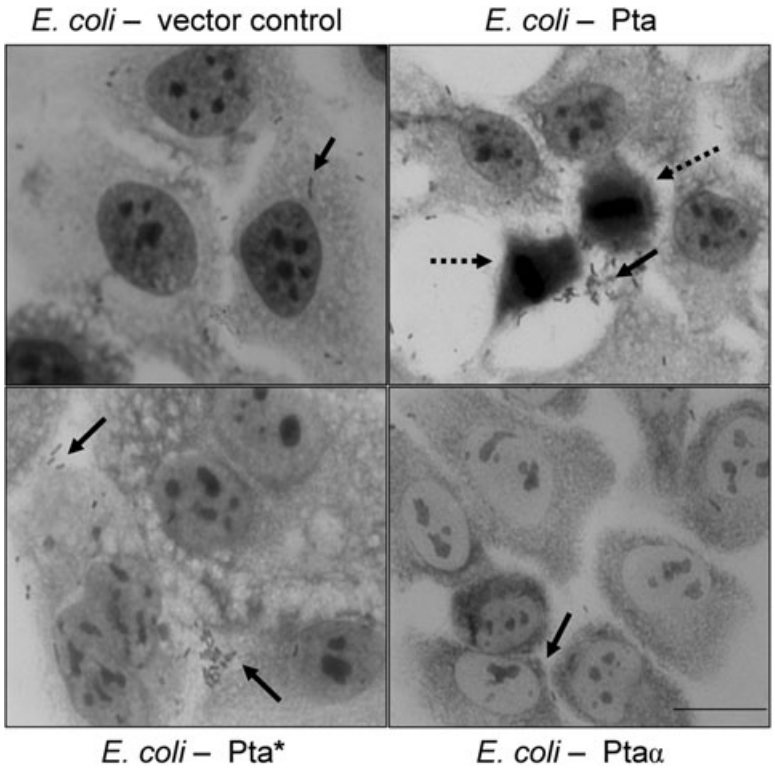

Fig. 3. Interaction of *E. coli* BL21plysS with human bladder epithelial cell monolayer. UMUC-3 cells were cultured as a monolayer on poly L-lysine-treated coverslips and were infected with *E. coli* BL21plysS expressing pET21A vector alone as control; Pta (*E. coli*-Pta); $Pta_{(S366A)}$ (*E. coli*-Pta*); or Pta-α (*E. coli*-Pta-α). Giemsa-stained cells were imaged at 100× magnification. Solid arrows indicate bacterial cells and dashed arrows point to the lysed host cells. Bar = 100 μM.

E. coli BL21 and were detected in the soluble fraction, but not in the OM fraction of the cell (Fig. 2B). This suggested that the entire beta domain is required for the OM translocation of the protein, and that the truncated versions of the beta domain do not adopt an oligomeric form to perform this function. Furthermore, the inability of even the shortest truncation at amino acid residue 1054 (T-1054) or the mutated 1072* version to successfully transport the passenger domain to the OM reiterates the significance of the hydrophobic residues in the C-terminus of the AT in forming an anchor to the OM.

Interaction of Pta-expressing E. coli *BL21 with human bladder epithelium* in vitro

Pta appears as a stable 110 kDa protein in both its OM-associated and in its purified form. This led to the hypothesis that Pta may act either as an agglutinin or as an adhesin as seen in case of Hia, TibA, YadA, and other similar ATs where the alpha domain is not cleaved from the beta domain in the OM (Klemm *et al*., 2006; Girard and Mourez, 2006). To determine a possible role for Pta in the virulence of *P. mirabilis*, we adopted a gain-of-function approach and infected human bladder epithelial cells independently with *E. coli* BL21 expressing vector alone, wild-type Pta, the serine protease mutant $Pta_{(S366A)}$ or the alpha domain (Pta-α). We observed cell–cell aggregation of *E. coli*-Pta cells as shown in Fig. 3B (solid arrow). Aggregation was also seen among *E. coli*-$Pta_{(S366A)}$ cells (Fig. 3C, solid arrow), suggesting no role for protease activity in this process. This phenotype, however, was not observed with either *E. coli* BL21 expressing the vector control or Pta-α, confirming that the phenotype is Pta dependent and that its OM localization is essential. Also, we observed no increase in adhesion of *E. coli* BL21-Pta cells to the bladder epithelial cells (when compared with vector control), and repeated attempts to quantify the *E. coli*-Pta recovered from the infected monolayer were unsuccessful, suggesting Pta does not mediate adhesion of the bacterium to the host cell. Indeed, in many cases the recovery of *E. coli*-Pta was many folds lower than that of *E. coli*-$Pta_{(S366A)}$ or *E. coli*-pET21A (data not shown).

Surprisingly, in addition to the autoaggregation phenotype, infection of tissue culture with *E. coli* BL21-Pta resulted in the condensation of the bladder cell cytoplasm, detachment from the surface and cell lysis (Fig. 3B, dotted arrow), suggesting a toxin-like activity associated with Pta. This phenotype was specific to wild-type Pta and was not observed with *E. coli* BL21 vector control (Fig. 3A) or either of the Pta variants (active-site mutant or passenger domain alone) (Fig. 3C and D). We observed a very rare incidence of vacuole formation (in less than 5% of cells) in the host cell cytoplasm when infected with *E. coli*-$Pta_{(S366A)}$, but this was not consistently observed when the infections were repeated with either whole cell or the purified $Pta_{(S366A)}$. Quantification of lactate dehydro-

genase release (as a measure of bladder cell lysis) when infected with each of the *E. coli* strains was also performed using incubation with Triton X-100 and *E. coli* expressing vector only as controls. *E. coli* expressing Pta lysed 70% of bladder epithelial cells, whereas *E. coli* expressing Pta* and *E. coli* expressing Pta-α resulted in lysis of only 18.3% and 11% cells, respectively, above the background (data not shown). The data further confirmed the interpretations made from microscopic analysis.

In these initial observations Pta demonstrated a combination of two distinct phenotypes that has not been reported in any AT studied so far: Pta promoted cell–cell aggregation of the bacterium and, when in interaction with the host, elicited a cytopathic effect. Both of these features have strong implications for the pathogenesis of *P. mirabilis* infection as this bacterium is known to form efficient biofilms on catheters that aids in the long-term persistence of the infection in the host (Stickler *et al.*, 1993).

Time- and dose-dependent lysis of bladder cells by Pta

Cytopathic effects of ATs such as Sat (Guyer *et al.*, 2002), Pet (Navarro-Garcia *et al.*, 2007) and EspC (Navarro-Garcia *et al.*, 2004) is shown to be associated with their protease activities. To estimate the cytotoxic effects of Pta quantitatively, we determined the time-course of Pta-mediated bladder cell lysis. Bladder epithelial cells were incubated with increasing concentrations (0–8 μg ml^{-1}) of Pta, or each of its active-site mutants (Pta$_{(S366A)}$ or Pta$_{(S366A/H147A)}$) and release of soluble LDH into the culture supernatant was used as an index of cell lysis. Figure 4A illustrates the extent of host cell lysis using various concentrations of Pta, with maximum lysis measured upon incubation with 8 μg ml^{-1} (7.2 nM) for 120 min. In agreement with the predicted catalytic role of Ser366 and His147, the ability of the active-site serine mutants Pta$_{(S366A)}$ and Pta$_{(S366A/H147A)}$ to lyse the host cells was reduced to about 20% of that of the wild-type Pta (Fig. 4A) in the same time period tested. Indeed, incubating bladder cells with 15 nM of each of the mutant proteins for longer incubation period (up to 16 h) did not result in any significant increase in the overall lysis of the bladder cells (data not shown).

To determine the mode of host cell damage induced by Pta, cells treated either with buffer control or with Pta (8 μg ml^{-1} or 7.2 nM) were microscopically examined at various time intervals. Cytotoxicity was first observed at 30 min after toxin addition (Fig. 4B; bottom row); alteration of the host cell morphology due to membrane damage was followed by leakage and condensation of the cell cytoplasm at 60 min, and breakdown of the cell components, resulting in lysis and detachment from the surface ensured after 90–120 min of incubation (Fig. 4B; bottom row). This phenotype was not observed in cells incubated with phosphate-buffered saline (PBS) for the same time intervals (Fig. 4B, top row).

Expression and purification of the passenger domain

We cloned the putative passenger domain (residues 1–730) of Pta and affinity purified a ~75 kDa Pta-α-6X-His to > 95% homogeneity from the soluble fraction of *E. coli* BL21 (Fig. 5A and B) and the protein identity was confirmed by mass spectrometry. Pta-α also appeared as both pre- and catalytically mature protease with the latter being the predominant form (Fig. 5B). The two active-site mutants of Pta-α, Pta-α$_{(S366A)}$ and Pta-α$_{(H147A)}$ were also purified by similar procedure and the pre-, as well as mature subtilase was observed in each case when stained with Anti-Pta antisera (Fig. 5C). N-terminal sequence of the mature ~75 kDa protein determined in each case aligned with that of the mature ~110 kDa Pta suggesting a similar secondary processing event. Comparison of the OM protein profiles of *E. coli* expressing vector alone (as control) with that expressing Pta-α both by Commassie stained gel (Fig. 5B) and by immunoblot analysis (Fig. 5C) showed no indication of Pta-α in the OM of the cell. This confirms our earlier prediction that the C-terminal amino acid residues 730–1072 of Pta form the translocator domain and are essential for the transport of Pta across the OM.

Protease activity of the putative subtilase, Pta

The presence of conserved catalytic residues in Pta and other subtilase-like enzymes such as SubA, Fls and PspA suggested that Pta may possess a protease-like activity associated with the alpha domain of the AT. Consequently, we probed the substrate specificity and optimum conditions for protease activity of purified Pta-α (passenger domain) towards various synthetic *p*-nitroanilide substrates (see *Experimental procedures*). Pta-α hydrolysed only chymotrypsin-specific substrates as indicated by the hydrolysis of *p*-nitroanilides with phenylalanine and leucine residues at the P1 position (Fig. 6A) with much greater affinity, but did not catalyse the hydrolysis of substrates with arginine, valine or alanine at that position to any appreciable extent (Fig. 6A). The protease activity was greatly diminished either by changing the Ser366 ($P < 0.01$) or His147 ($P < 0.05$) to alanines or by treating the protease either with PMSF (phenyl-methylsulphonyl fluoride) (Fig. 6A and B and Table 1) or with DFP (diisopropyl flourophosphate) (Table 1), suggesting the significance of Ser366 and His147 in catalysis. However, inhibition of protease activity was greater in S366A point mutation than that observed in H147A mutant. The rates of the reaction of Pta-α for substrate S1 were approxi-

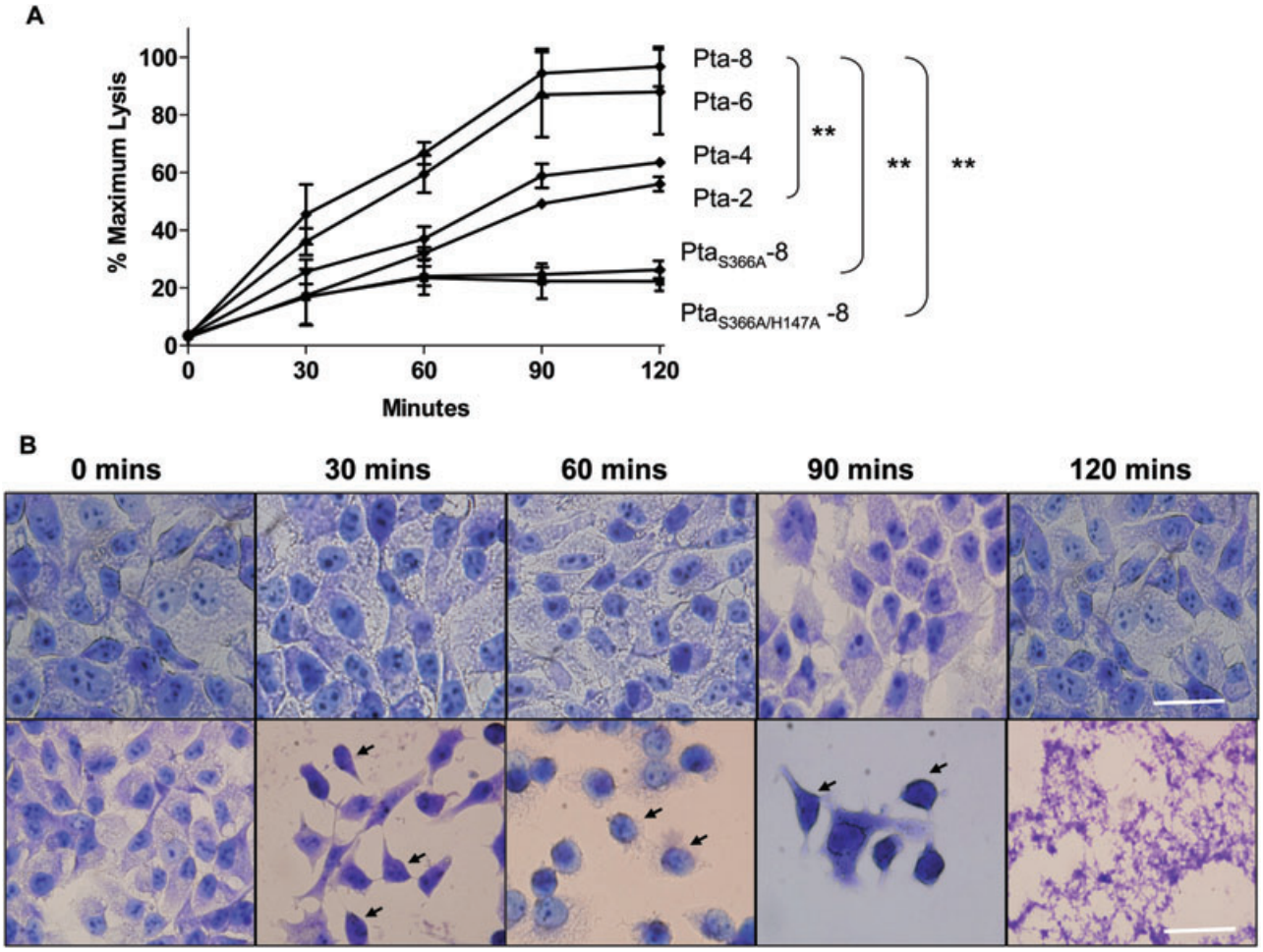

Fig. 4. Interaction of purified Pta with bladder epithelial cell monolayer.
A. Time- and dose-dependent lysis of UMUC-3. UMUC-3 cells were cultured to 80% confluence in tissue culture-treated 96-well plate and infected independently with known concentrations of Pta, Pta* or Pta$_{(S366A/H147A)}$. Extent of lysis by Pta is represented as a per cent of maximum bladder cell lysis by Triton X-100 treatment. Data are mean ± SE obtained from three independent studies each performed in triplicate. $^{**}P < 0.01$. Pta-8, Pta 8 μg ml^{-1}; Pta-6, Pta 6 μg ml^{-1}; Pta-4, Pta 8 μg ml^{-1}; and Pta-2, Pta 2 μg ml^{-1}; Pta$_{(S366A)}$-8, 8 μg ml^{-1} Pta (Ser366Ala) active-site mutant; and Pta$_{(S366A/H147A)}$-8, 8 μg ml^{-1} Pta (Ser366Ala/His147Ala) active-site double mutant.
B. Qualitative estimation of cytotoxicity. UMUC-3 cells were treated either with PBS + 0.05% zwittergen (top) or with 8 μg ml^{-1} Pta (bottom) and images were taken after staining with Giemsa. Bladder cells treated with Pta for 120 min were not subjected to extensive washes to prevent complete loss of lysed cells from the glass surface. Arrows point to lysed bladder cells. Images are taken at 60× magnification. Bar = 100 μm.

mately 35 and 25 times higher than that the S366A and H147A variants respectively. An analysis of the enzyme and substrate kinetics showed that Pta cleaves *N*-Suc–Ala–Ala–Pro–Phe–*p*Na with a $K_M = 22$ μM (Fig. 6C) and *N*-Suc–Ala–Ala–Pro–Leu–*p*NA with a $K_M = 31$ μM (data not shown). However, specific substrates for other serine proteases, such as BA*p*Na (trypsin), *N*-Suc–Ala–Ala–Ala–*p*Na (Fig. 6A) and *N*-Suc–Ala–Ala–Pro–Val–*p*Na (data not shown), were not cleaved by *P. mirabilis* Pta-α.

A range of synthetic as well as naturally occurring inhibitors was used to determine the nature of the active site of Pta-α. Protease activity was inhibited ~90% by treating either with PMSF or with DFP, indicating the role of Ser and His residues as the catalytic residues (Fig. 6A). In accordance with our prediction, inhibitors of cysteine-proteases did not affect its activity (Table 1); these results taken together classify Pta as a serine protease. Some inhibitors are instrumental in determining the inhibitor P1 positions, and also help in determining the enzyme specificity. We employed the microbial-derived inhibitors leupeptin and chymostatin that are specific to serine and thiol proteases and found complete inhibition of the protease activity (Table 1). In addition, inhibitors such as STI (soybean trypsin inhibitor) and BBI (Bowman-Birk trypsin inhibitor) that are specific against subtilisin-like enzymes showed up to 60–70% inhibition, whereas the trypsin-specific inhibitors TLCK (*N*-alpha-*p*-Tosyl-L-lysine-chloromethyl ketone hydrochloride) and TPCK (*N*-alpha-*p*-Tosyl-L-phyenylalanine chloromethyl ketone) had only moderate or no effect respectively (Table 1). Together the

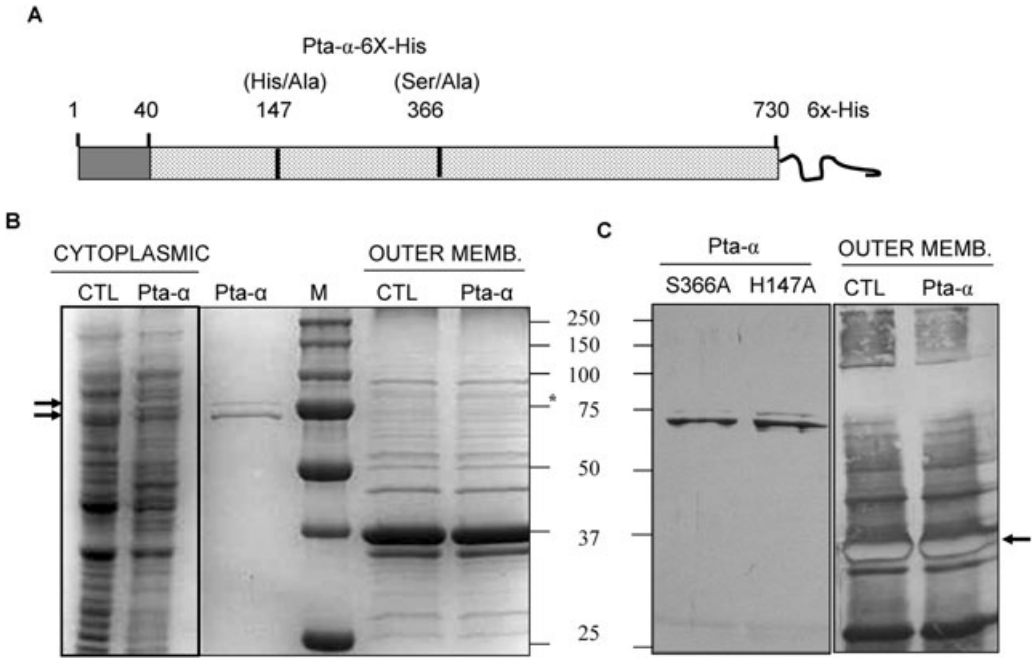

Fig. 5. Structure of Pta-α and purification.
A. Schematic of various constructs of Pta-α. The 730-amino-acid-long alpha or passenger domain of Pta; Pta-α, active-site mutants Pta-$\alpha_{(S366A)}$ or Pta-$\alpha_{(H147A)}$ were each cloned into pET21A and overexpressed as a C-terminus 6X-His-tagged fusion protein in *E. coli* BL21plysS.
B. Purification of Pta-α. Pta-α was overexpressed in *E. coli* BL21plysS. Pre- and mature forms of ~75 kDa Pta-α in the soluble protein fraction or in their purified form are identified by arrows. Protein fraction from *E. coli* BL21plysS expressing the vector alone serves as the control (CTL). The last two lanes show the OM protein fraction; the possible position of Pta-α is shown by the asterisk.
C. Immunoblot of Pta-α and OM fractions. Purified active-site variants of the passenger domain Pta-α (S366A) and Pta-α (H147A), 6 μg of OM protein each from *E. coli* expressing pET21A (CTL) and *E. coli* expressing Pta-α (Pta-α) were run on a 10% SDS-PAGE, transferred onto a nitrocellulose membrane and stained using polyclonal Anti-Pta antisera (1:750) and Goat Anti-Rabbit IgG-HRP conjugate (1:10000). Arrows at 75 kDa marker identify pre- and mature forms of Pta-α and the lower arrow at ~30 kDa indicates OmpA protein used as a marker for OM (negatively stained). M = molecular size marker.

substrate specificity and the inhibitor profile confirm Pta as a subtilisin-like serine protease.

Cytoplasmic urease activity of *Proteus* and the accumulation of bicarbonate as well as ammonium ions results in an alkaline micro-environment surrounding *P. mirabilis* in the human urinary tract (Mobley and Warren, 1987). As Pta is a surface-expressed protease, we hypothesized that pH may play a significant role in the function of this protease. To determine the pH-dependent stability as well as the optimum pH for Pta activity, we pre-incubated Pta-α in carbonate buffer in a range of pH 5–11 spanning acidic, neutral and alkaline conditions and then tested its activity against its specific substrate *N*-Suc–Ala–Ala–Pro–Phe–*p*Na. Pta demonstrated maximum substrate hydrolysis between pH 8.5 and 9.0 and the activity was reduced by at least 40% either under neutral (pH 7.0) or under higher alkaline conditions of pH 9.5 and 10 (the latter case might result in the precipitation of the protein due to the presence of Ca^{2+}-binding pocket). However, a significant loss of protease activity was observed in the acidic range (pH 5–6) (Fig. 6B), although the protein was resistant to acidic degradation as seen using gel electrophoresis (data not shown). We hence classified Pta as a subtilisin-like alkaline protease.

Cytotoxicity is associated with the passenger domain

As for other characterized ATs, the passenger or alpha domain (Pta-α) of Pta contains all catalytic residues required for substrate hydrolysis. To test the hypothesis that the alpha domain is sufficient for cytotoxicity, we tested the activity of Pta-α and each of its active-site mutants over a range of kidney and bladder cell lines. As expected, incubation with purified Pta-α (8 μg ml^{-1} or 9.2 nM for 120 min) resulted in complete lysis of human kidney (HEK293), bladder cells (UMUC-3) and Vero monkey kidney cells as indicated by the measured LDH release (Fig. 7A). In accordance with the enzymatic activity, cytotoxicity of the active-site mutants (S366A and H147A) and PMSF-treated Pta-α was significantly ($P < 0.01$) reduced (Fig. 7A). However, both hamster kidney (BHK21) and mouse kidney (MMK-5) cell lines showed moderate resistance against Pta-α activity (Fig. 7A). These results confirmed that the alpha domain of Pta is

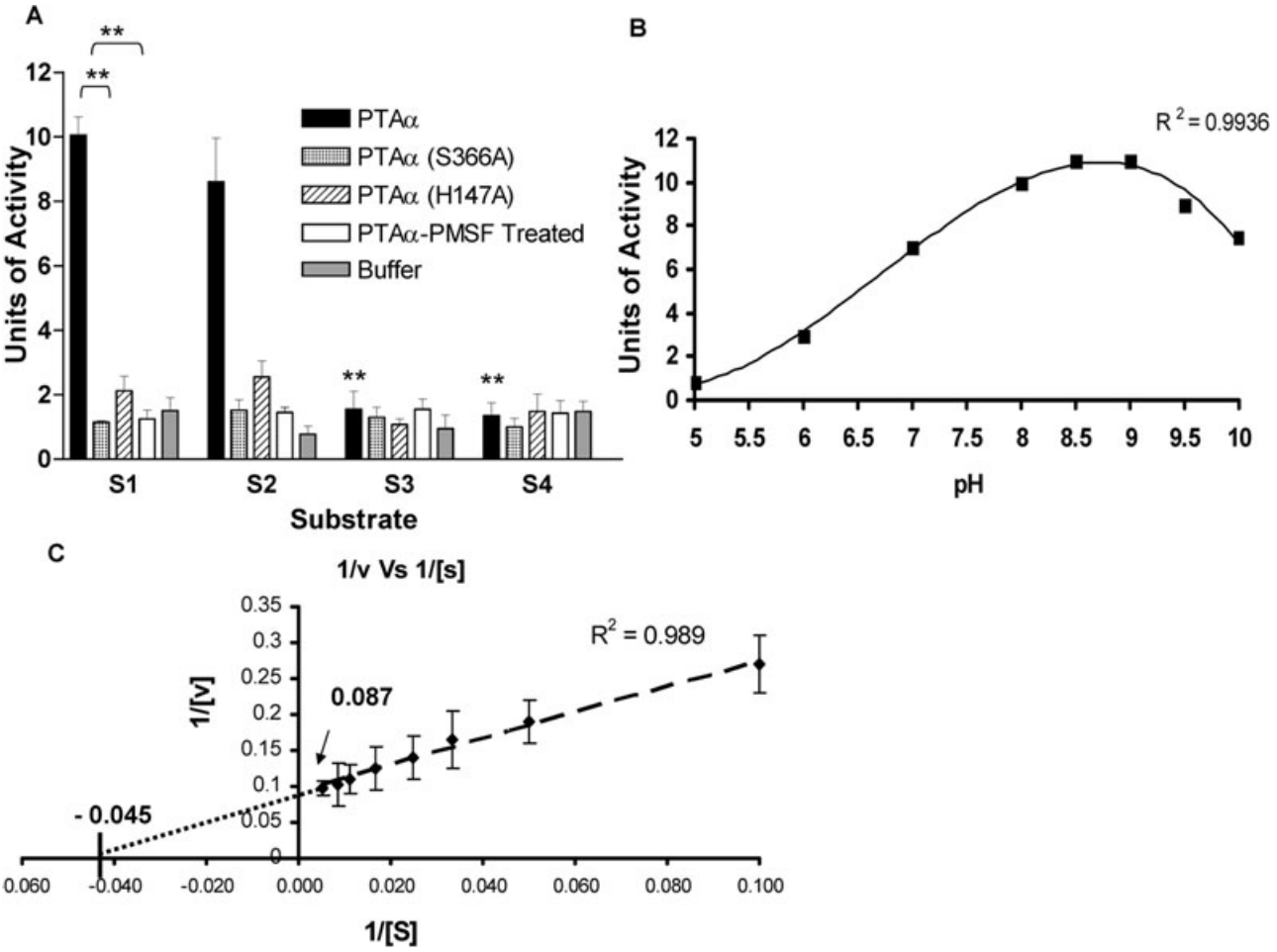

Fig. 6. Protease activity of Pta.
A. Substrate specificity and active-site determination. Proteases (20 nM Pta-α, Pta-$\alpha_{(S366A)}$, Pta-$\alpha_{(H147A)}$ and Pta-α-PMSF inactivated) were assayed against 100 μM of each substrate, S1: *N*-Suc–Ala–Ala–Pro–Phe–*p*Na; S2: *N*-Suc–Ala–Ala–Pro–Leu–*p*Na; S3: Benzoyl–Arg–*p*Na; and S4: *N*-Suc–Ala–Ala–Ala–*p*Na in 50 mM $NaPO_4$ buffer, pH 8.3, containing 20 mM $CaCl_2$ and 0.005% Triton X-100. The protease activity of Pta-α was significantly (**$P < 0.01$) higher than the protease activity of each of the point mutants or the PMSF-inactivated protease. One unit of protease activity = nmol substrate hydrolysed per minute per milligram of protein.
B. The pH optimum for protease activity of Pta-α (20 nM) was determined using S1 (100 μM), in the assay buffer with a range of pH. One unit of protease activity = nmol substrate hydrolysed per minute per milligram of protein.
C. K_M for S1 was determined by using 20 nM Pta-α and a range of substrate concentrations (10–150 μM) at pH 8.5. v = nmol substrate hydrolysed per minute.

the active protease and is responsible for the cytotoxicity of Pta.

Pta-α induces actin depolymerization and destabilizes nuclear membrane integrity

Vero cell lines were independently incubated with PBS + 0.05% zwittergen, and either wild-type Pta-α, Pta-$\alpha_{(S366A)}$, or PMSF-treated Pta-α (Fig. 7B) for 60 min to closely monitor the initial events in host cell damage. Cells were subsequently stained with the FITC-phalloidin and DAPI to visualize actin and nuclei respectively. Vero cells incubated with wild-type Pta-α (Fig. 7B, the second panel) showed membrane disruption leading to release of cytoplasmic contents indicated by the dispersion and degradation of actin filaments (indicated by arrows). Consequently, this also affected the nucleus as the DNA was stained more lightly in Pta-α intoxicated cells than in the cells treated with either of the protein variants or with buffer control (Fig. 7B). Upon longer incubation (up to 2 h) we observed complete loss of actin staining and the cytoplasm was condensed to the walls of the nuclei. The nuclei too were stained very lightly and lost their structural integrity (data not shown). Although, to our knowledge, this is the first report of nuclear damage induced by a cytotoxic AT, we predict that it is an indirect consequence due to certain downstream cellular events in the host rather than a direct effect of Pta.

Table 1. Effect of selected inhibitors on the Proteinase activity of Pta.

Inhibitor[a]	% Proteinase activity[b]
PMSF	10
DFP	5
TLCK	100
TPCK	60
STI	30
BBI	40
Chymostatin	10
Leupeptin	0

a. Pta was allowed to complex with an inhibitor (concentration subject to the nature of the inhibitor). After pre-incubation for 30 min, the residual protease activity was measure towards 100 μM *N*-Suc–Ala–Ala–Pro–Phe–*p*Na.
b. Relative to Proteinase activity under optimum conditions of pH (8.5), temperature (37°C), substrate and native enzyme concentrations (100 μM and 50 nM respectively).

Induction and stability of Pta

Environmental factors such as temperature, osmolarity, pH and metal ions have been shown to influence the expression of various virulence factors. Even though evidence of regulators controlling the expression of AT is minimal (Tukel *et al*., 2007), external factors such as mentioned above were proven to regulate the expression of ATs (Henderson *et al*., 1999). To determine the factors that either induce the expression of or stabilize Pta at the OM, *P. mirabilis* HI4320 was cultured in LB under various conditions (see *Experimental procedures*) and protein expression was detected by immunoblotting. Table 2 lists the conditions and their effects on the expression of Pta in *P. mirabilis*. Pta expression was twofold higher at 37°C than at 25°C, a feature expected with virulence determinants in pathogens. Pta was moderately repressed under the conditions of iron starvation or high salt where the cellular resources are mainly channelled towards upregulation of iron receptors present in the OM. Interestingly, expression of Pta was induced about two- and threefold when the bacteria were cultured in alkaline conditions or in medium supplemented with calcium ions, respectively, but not in the presence of Mg^{2+} (Fig. 8; Table 2). Gene expression at the transcript level was also determined using quantitative reverse transcription polymerase chain reaction (RT-PCR) assay (Fig. 8B). The *pta* gene was upregulated at least three- to fourfold when cultured in alkaline conditions of pH 9.0 or at 37°C (Fig. 8B) and downregulated when the pathogen was grown under acidic pH (5.0) or at lower temperatures (25°C) (Fig. 8B). Addition of Fe^{2+} or Mg^{2+} ions resulted only in a moderate to no increase in gene expression at either pH 7.0 or 9.0, whereas addition of Ca^{2+} showed moderate increase only at pH 7.0 but not at pH 9.0. We hence concluded that unlike iron and magnesium, presence of calcium to alkaline environment helps Pta maintain a stable conformation in the OM. These results suggest that *P. mirabilis* adapts to the conditions in its immediate environment in the liquid culture and regulates or stabilizes its key OM virulence factors to facilitate infection.

Inactivation and complementation of pta *in* P. mirabilis *HI4320*

To assess the role of Pta in the virulence of *P. mirabilis*, we constructed a *pta*-deficient (*pta*Ω*aph*A3) strain of HI4320 using Targetron®. A kanamycin cassette was inserted towards the 5′ end (encoding the N-terminal passenger domain) of the gene resulting in the complete loss of protein expression. Insertional inactivation of *pta* was confirmed both by PCR (data not shown) and by immunoblots using polyclonal Anti-Pta antiserum (Fig. 9A). The mutant was complemented *in trans* by either the wild-type *pta* gene (resulting in full cytotoxicity) or the S366A active-site variant (diminished cytotoxicity) expressed under the control of an inducible promoter (see *Experimental procedures*). Expression and OM localization of Pta in the complemented strain was confirmed using immunoblots (Fig. 9A); no trace of Pta was seen in the concentrated supernatants (data not shown). Growth kinetics of the mutant were very similar to that of the wild-type when tested in LB, DMEM, M9 and urine, both at 37°C and at 25°C (data not shown), suggesting no role for Pta in nutrient or ion transport across the OM.

Characterization of Pta in P. mirabilis *HI4320*

The first indication of Pta-mediated cell–cell aggregation of *E. coli* BL21 was seen when the bladder cells were infected with *E. coli* BL21 expressing Pta (Fig. 3). We asked if a similar phenotype can be associated with Pta in *P. mirabilis*.

Evidence of cytotoxicity. We tested the relative abilities of *P. mirabilis* HI4320 (WT), the isogenic mutant *pta*Ω*aph*A3, WT overexpressing Pta (WT/pBAD-*pta*), or the mutant overexpressing either the WT-Pta or its active-site serine mutant S366A (see *Experimental procedures*) to lyse bladder epithelial cells using LDH release as an index of cytotoxicity. Infection with 10^7 colony-forming units (cfu) of the strain overexpressing Pta resulted in complete lysis of the host cells in 4 h compared with about 50% lysis by 10^7 cfu of WT HI4320 in the same time period correlating this phenotype to the protease activity of Pta ($P < 0.01$) (Fig. 9B). Cytotoxicity was attenuated using whole washed cells of the isogenic *pta* mutant of HI4320 ($P < 0.05$), and was restored to the wild-type levels only when provided with WT Pta but not with $Pta_{(S366A)}$ ($P < 0.05$). The extent of bladder cell lysis was very similar (~25% of the

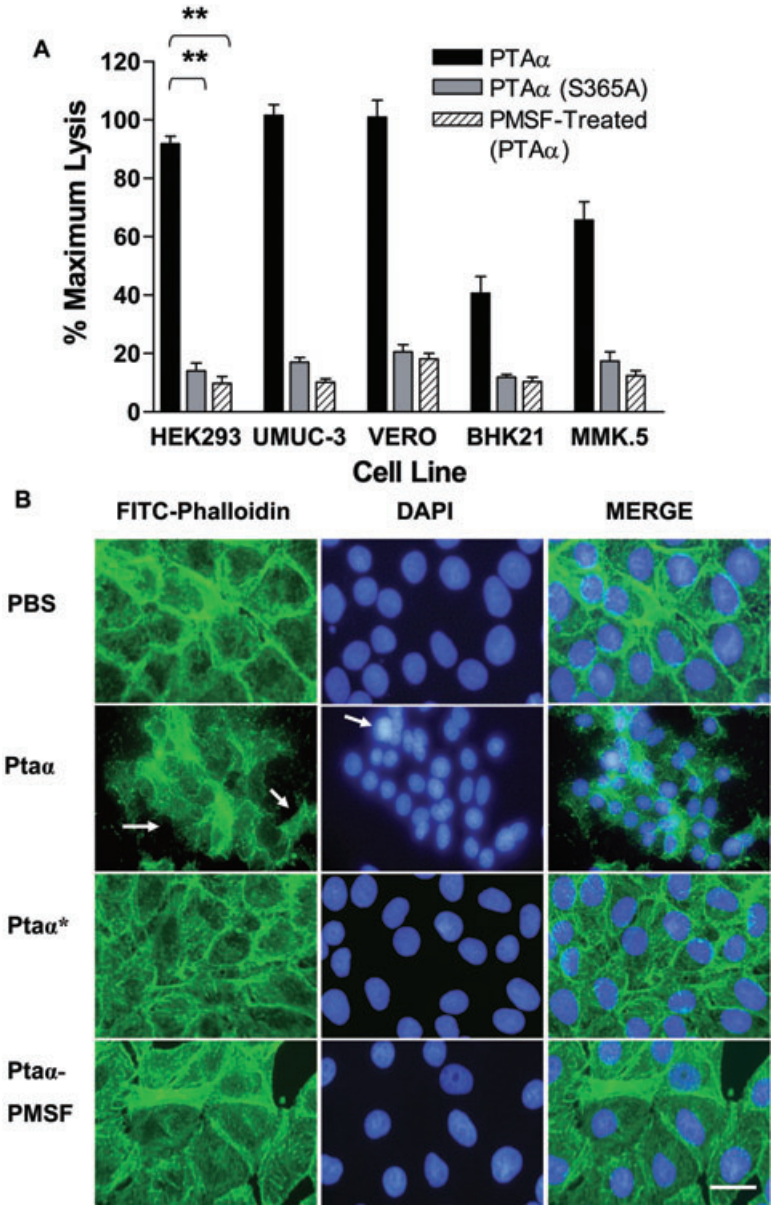

Fig. 7. Cytotoxicity of Pta-α on cell lines.
A. Interaction of Pta-α with various host cell lines. Confluent host cell lines were treated with 8 μg ml^{-1} Pta-α, Pta-α$_{(S366A)}$ or Pta-α (inactivated with PMSF) for 120 min and the release of intracellular LDH by the host cells was measured. Extent of host cell lysis by the protein is represented as a per cent of maximum lysis by Triton X-100 treatment, normalized with values obtained from buffer treatment alone. Mean ± SE obtained from three independent studies each performed in triplicate is shown (**$P < 0.01$).
B. Immunofluorescent detection of host cell damage. Confluent monolayer of Vero kidney cell line was treated with of PBS + 0.05% zwittergen; 8 μg ml^{-1} each of Pta-α; Pta-α inactivated with PMSF; and Pta-α$_{(S366A)}$ (Pta-α*). Representative images of cells stained with FITC-phalloidin, DAPI and merge are shown. Arrows indicate actin degeneration in infected cells. Magnification = 100×; bar = 100 μm.

Pta-induced lysis), however, when infected with the concentrated supernatants of each strain suggesting this is a Pta-independent event (mediated by haemolysin or other cytotoxic proteins in *P. mirabilis*), as well as confirming the location of Pta to the OM of the pathogen. Similar extent of host cell lysis in the supernatants together with basal cytotoxicity exhibited by the mutant strain indicates the presence of other secreted or OM-associated toxic proteases in *Proteus*.

Evidence of autoaggregation. In a similar fashion, the ability of all the above strains to autoaggregate was also assessed. All strains were individually re-suspended in phosphate buffer (pH 8.5) to a cell density of about 460–480 Kletts and density was measured at different time intervals. Wild-type strain HI4320 showed moderate autoaggregation with approximately 60% reduction in cell density over 300 min incubation. As hypothesized, the rate of autoaggregation was significantly increased in the wild-type strain overexpressing Pta, with the bacterial cell density decreasing significantly after the first 120 min and with no significant decrease after about 240 min (Fig. 10). Conversely, the rate of autoaggregation was significantly reduced in *pta*Ω*aph*A3 strain in the same time period. However, this phenotype was restored in the mutant strain overexpressing either the wild type or the active-site serine mutant of Pta (Fig. 10). These results suggested that under the optimum conditions of protein expression, pH and cell density, *P. mirabilis* can autoaggregate and that Pta is perhaps one of the key proteins that promote

Table 2. Effect of selected conditions on the expression of Pta.

No.	Condition of growth[a]	Fold change in expression[b,c]
1	Exponential phase of growth	2
2	25°C	–3
3	42°C	–
4	Acidic (pH 5.0)	–3
5	Alkaline (pH 9.0)	2.5
6	0.5 M NaCl	–2
7	20 mM $CaCl_2$	3
8	$MgCl_2$ (0.5, 1, 2 mM)	–
9	Iron chelation (15 μM desferral)	–2
10	Excess iron (0.5 mM $FeSO_4$)	–

a. *P. mirabilis* HI4320 cultured under different conditions or harvested at different growth phases.
b. OM protein was stained with Anti-Pta antibody to estimate the amount of protein expressed.
c. Relative to protein expressed in the culture grown at 37°C, pH 7.0, harvested at the late log early stationary phase of growth.
–, no change.

this phenomenon. Interestingly, even though Ser366 is essential for catalysing substrate hydrolysis and cytotoxicity, alteration of this residue did not influence the process of autoaggregation. The data here confirm the bi-functional nature of the AT Pta in *P. mirabilis*, demonstrating a unique phenotype combination of bacterial cell–cell aggregation and OM-associated cytotoxicity.

Role of Pta in the virulence of P. mirabilis. Pta was first identified in our laboratory as one of the OM surface-expressed proteins of *P. mirabilis* recognized by antisera from mice chronically infected with *Proteus* (G.R. Nielubowicz and H.L.T. Mobley, unpubl. data). This was a preliminary indication that this protein was expressed during infection of the host. We performed co-challenge experiments where mice were infected with equal numbers of parental strain HI4320 and its isogenic *pta* mutant (2.5×10^7 of each strain) and tested the relative abilities of each strain to colonize the urinary tract and the spleen of mice. The *pta*Ω*aph*A3 strain was significantly outcompeted by the parent strain in the bladder ($P < 0.05$) and both the kidney and spleen ($P < 0.01$) (Fig. 11). In five

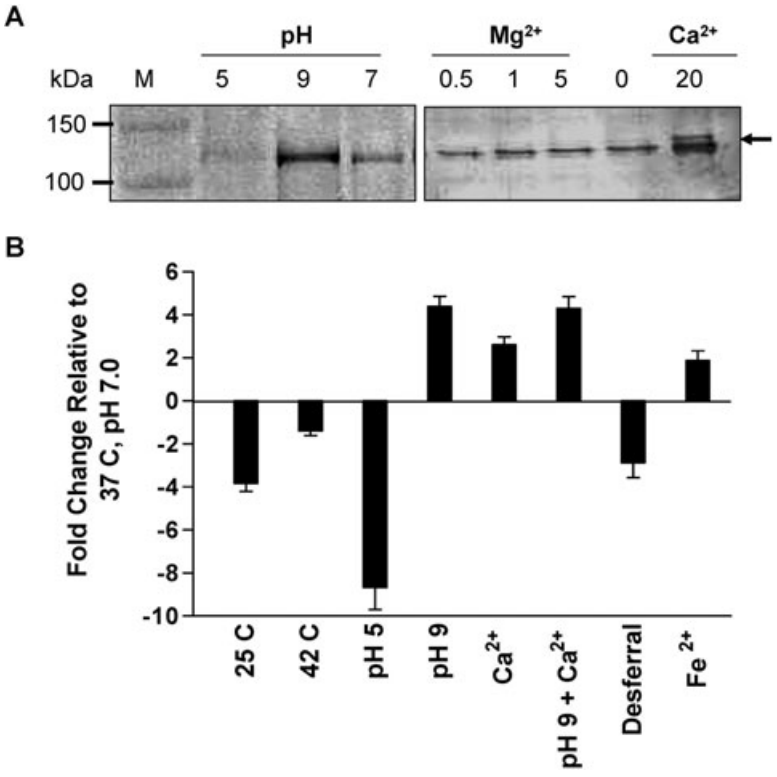

Fig. 8. Induction of Pta.
A. *P. mirabilis* HI4320 was cultured in LB under different conditions and the outer membrane fraction (6 μg) from each was electrophoresed on a 10% SDS-PAGE. Concentrations (in mM) for Mg^{2+} and Ca^{2+} are given. Immunostaining was performed with Anti-Pta antiserum (1:750) and Goat Anti-Rabbit IgG-AP conjugate (1:10 000). Density of each band was estimated using ImageJ software. Arrow identifies Pta in each lane. The upper minor band in Ca^{2+} lane is the pre-protease form of Pta.
B. Quantitative PCR for *P. mirabilis* HI4320 *pta*. Fold change in *pta* expression when cultured in various conditions of temperature, pH and metal ion supplementation or iron chelation is given. Data were normalized to *rpoA* (DNA-dependent RNA polymerase Alpha) expression levels, and changes were determined by using LB medium (37°C, pH 7.0) as the calibrator.

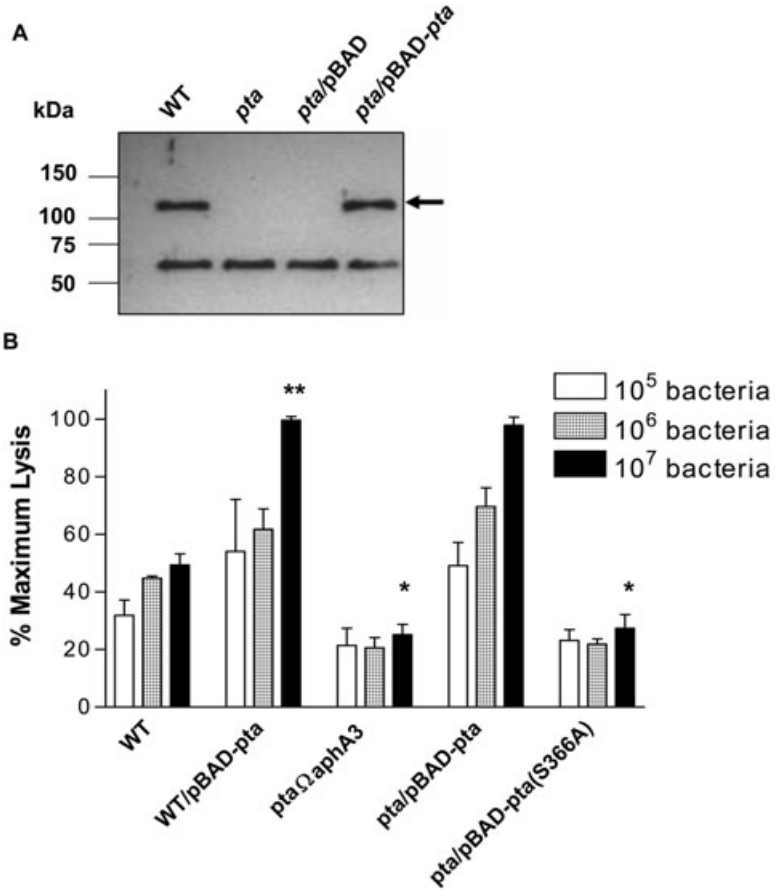

Fig. 9. Role of Pta in *P. mirabilis*.
A. Detection of Pta in wild type, mutant and complemented strain. OM fractions (6 μg) from each strain were electrophoresed on a 10% SDS-PAGE and immnoblotted with Anti-Pta antiserum (1:1500) and Goat Anti-Rabbit IgG-HRP conjugate (1:20 000). Arrow indicates immuno-stained Pta in each case. The ~65 kDa non-specific band was used as the loading control.
B. Infection of bladder cells with *P. mirabilis*. *P. mirabilis* was cultured until mid-exponential phase ($OD_{600} = 0.6$) in alkaline LB (pH 8.5) supplemented with $CaCl_2$ and 5% glycerol and was induced for 3 h with 5% arabinose (where appropriate). Confluent bladder epithelial cells were infected with different cell counts of *P. mirabilis* for 4 h. Extent of bladder cell lysis by whole cells of *P. mirabilis* is represented as a per cent of maximum cell lysis by Triton X-100 treatment. Data are represented as mean ± SE of three independent experiments, each conducted in triplicate. Significant differences (in bladder cell lysis) when compared with the treatment with 10^7 wild-type bacteria are indicated by $^*P < 0.05$; $^{**}P < 0.01$. WT: *P. mirabilis* parent strain; WT/pBAD-*pta*: *P. mirabilis* HI4320 strain overexpressing *pta*; *pta*: *pta*Ω*aph*A3; *pta*/pBAD-*pta*: *pta* expressing wild-type *pta* on pBAD; *pta*/pBAD-*pta*(S366A): *pta* expressing the active-site S366A mutant of *pta* on pBAD.

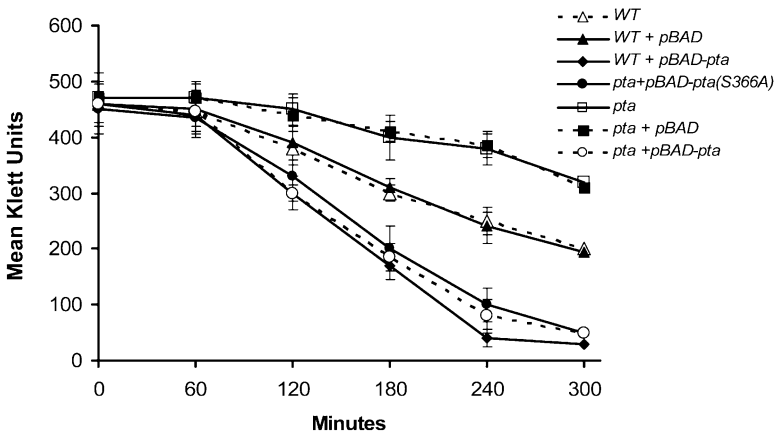

Fig. 10. Pta-dependent autoaggregation of *P. mirabilis*. Bacteria were cultured and induced (when appropriate) in a similar fashion. Bacteria were then re-suspended to a cell density of approximately 460–480 Klett units in phosphate buffer (pH 8.5) supplemented with $CaCl_2$. Data represent mean decrease in density of cell suspension (due to simultaneous increase in clumping and precipitation to the bottom of the tube) from three independent experiments. Difference in the Klett units at the end of 300 min incubation is significant between wild type and each of WT/pBAD-*pta* ($P < 0.01$), *pta*/pBAD-*pta* ($P < 0.01$), *pta*/pBAD-*pta*(S366A) ($P < 0.01$) and *pta* ($P < 0.05$). WT: *P. mirabilis* parent strain; WT/pBAD: WT expressing pBAD vector alone as control; WT/pBAD-*pta*: *P. mirabilis* HI4320 strain overexpressing *pta*; *pta*: *pta*Ω*aph*A3; *pta*/pBAD: *pta*Ω*aph*A3 expressing pBAD vector alone as control; *pta*/pBAD-*pta*: *pta* expressing wild-type *pta* on pBAD; *pta*/pBAD-*pta*(S366A): *pta* expressing the active-site S366A mutant of *pta* on pBAD.

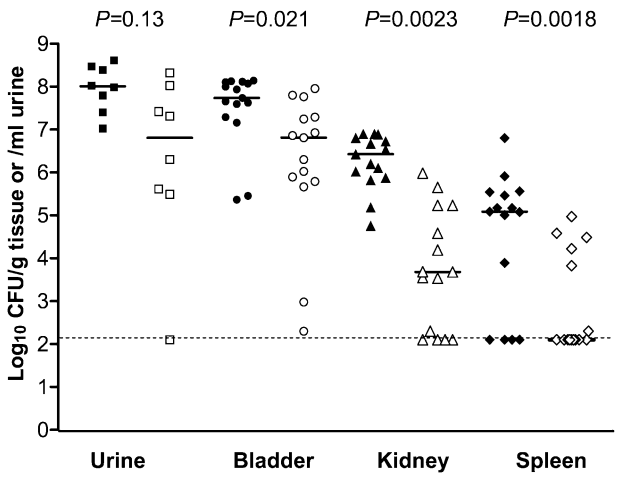

Fig. 11. Co-challenges of CBA/J mice with *P. mirabilis* HI4320 and the isogenic *pta* mutant. The assessment of virulence of *pta*Ω*aph*A3 in a CBA/J mouse model of ascending UTI, 7 days after co-challenge, with the parent strain. Each symbol represents $\log_{10}$ cfu per millilitre of urine or cfu per gram of tissue from an individual mouse. The solid symbols represent the wild-type counts and open symbols represent the counts of the *pta* mutant. The dotted line indicates the limit of detection. Solid black bars represent the median $\log_{10}$ cfu per millilitre of urine or cfu per gram of tissue, respectively, from a total of 15 mice for bladder, kidney and spleen and 10 for urine. Two-tailed *P*-values were determined by Wilcoxon matched pairs signed ranks.

of the 15 mice infected (with 1:1 ratio of wild type and *pta* strain of) *P. mirabilis*, the numbers of mutant bacteria were below the level of detection, strongly suggesting the mutant to be attenuated. Urine samples collected from five of the 15 mice in this study were contaminated and hence excluded from the data analysis. Of the remaining 10 mice tested for bacteria in urine, we found no significant difference between the wild-type and the mutant bacteria recovered from these samples ($P = 0.13$) (Fig. 11). This is the only cytotoxic AT protein affecting the colonization of a pathogen in its host, apart from the VacA in *Helicobacter pylori* (Salama *et al.*, 2001), inactivation of which compromises the ability of the mutant to colonize the host.

Discussion

Pta is an inducible subtilisin-like alkaline protease AT. Orf c2341 is annotated as a putative AT with a subtilisin motif (Pearson *et al.*, 2008). Subtilases are pre-protein convertases which, in eukaryotic cells, play a pivotal role in the processing of most precursor proteins in the secretory pathway (Steiner, 1998). In eukaryotes, these enzymes are themselves synthesized as pre-proteins and later undergo processing near their N-terminus, transforming them into catalytically active proteases (Seizen, 1996). However, such a phenomenon is rare in prokaryotes. Here we observe that *P. mirabilis* Pta exhibits a process similar to that seen in eukaryotes, with a longer pre-protein form (120 kDa) and an abundant shorter mature protease (110 kDa) (Fig. 1C). Even though a similar pattern was observed when overexpressed in *P. mirabilis* (data not shown), the abundance of the pre-protein form was much lower than that seen in *E. coli* BL21, suggesting an efficient processing of Pta in the native *Proteus* strain. Also this indicates that the shorter form is the catalytic protein. We expressed the full-length AT (Pta) and the passenger domain (Pta-α) in *E. coli* BL21 and affinity purified both proteins to > 95% homogeneity (Figs 1C and 5B). With the use of a broad range of substrates, inhibitors and assay conditions, we classified Pta as a protease belonging to the family of subtilisin-like alkaline serine proteases (Fig. 6 and Table 1). Active-site substitutions confirmed that an indispensable Ser366 and moderately critical His147 together with Asp533 form the catalytic triad of this protease, suggesting that other His or Asp residues that are in close proximity to the catalytic pocket may interact with Ser366 to transfer electrons during substrate cleavage; a feature usually found in subtilisin-like serine proteases (Seizen, 1996). This protease activity resides in the passenger domain and is also responsible for the cytotoxic activity of the protease. Residues 730–1072 form an approximately 30 kDa translocator domain which is essential in its native form for the OM localization of the AT (Fig. 5B).

The hallmark of a *Proteus* UTI is the formation of kidney and bladder stones, as well as catheter obstruction due to stone encrustation (Warren *et al.*, 1982; 1987; Mobley and Warren, 1987, Johnson *et al.*, 1993; Mobley, 1996b). Stone formation is due to the activity of the cytoplasmic urease that hydrolyses urea in the urine to CO_2 and ammonia; accumulation of the latter causes an increase in the pH and subsequent precipitation of magnesium ammonium phosphate (struvite) and calcium phosphate (apatite) crystals around the bacterium. Indeed, this alkalinized urinary tract would require that extracellular and surface-expressed bacterial proteins and enzymes have peak activity at the elevated pH that is maintained throughout a *P. mirabilis* infection. Here we demonstrate that temperature (37°C), pH (8.5–9.5), growth phase (exponential) and Ca^{2+} concentration (20 mM) are optimal for Pta expression in *P. mirabilis* (Fig. 8 and Table 2). These conditions simulate the environment that *P. mirabilis* encounters, and indeed creates, during infection of the urinary tract.

Pta is a bi-functional AT with both cytotoxin and auto-agglutinin activities. The subtilisin-like protease SubA of the AB_5 type toxin from STEC was the most recently discovered cytotoxic subtilisin identified in non-*Bacillus* species (Paton *et al.*, 2004). SubA internalizes into the eukaryotic host cell and inactivates a major chaperone BiP resulting in host cell lysis (Paton *et al.*, 2006). Here we

demonstrate the interaction of Pta (both in its cell-associated and in its purified form) leads to lysis of the cultured bladder epithelial cells (Figs 3, 4 and 7). Therefore Pta is the newest member of the group of cytotoxic ATs found in enteric pathogens. The mode of action of Pta, however, differs greatly from other known cytotoxic ATs such as Pet, Sat or VacA. Intoxication is mediated neither by formation of vacuoles in the host cytoplasm as induced by Sat (Guyer *et al*., 2002) and VacA (Harris *et al*., 1996), nor by the direct disruption of the cytoskeleton as seen in case of EspC or Pet (Navarro-Garcia *et al*., 1999; 2004). Repeated attempts to detect Pta in the host cell cytoplasm using fluorescent microscopy were unsuccessful, suggesting either that the mechanism of Pta action was external or that the amount of Pta internalized in the susceptible host cell is below the limit of detection. We hypothesize that Pta first punctures the host cell membrane leading to the leakage of cytosol. The loss of cell cytoplasm and the resulting osmotic stress perhaps then triggers the depolymerization of actin filaments (Fig. 7B). This may indirectly destabilize the nuclear membrane resulting in the loss of its structural integrity. The mode of action of Pta illustrates diverse ways in which ATs can intoxicate the host cell.

Autoaggregation is one of the prominent functions mediated by ATs and has been demonstrated for AIDA-1, Ag43, Cah and TibA (Klemm *et al*., 2006). Few of these agglutinins, however, exhibit dual or multiple functions such as the invasion of or adhesion to the host or to its extracellular matrix (Girard and Mourez, 2006). Here we demonstrate that Pta exhibits the bi-functional phenomenon by mediating the autoaggregation of bacterial cells and elicits cell damage when in contact with the host (Figs 3, 8B and C). That Pta mediates autoaggregation was clearly demonstrated in *P. mirabilis* HI4320 and was independent of its proteolytic activity catalysed by Ser366 (Fig. 10). It is, however, interesting to note that even though overexpression of Pta accelerated the rate of autoaggregation of *P. mirabilis*, the process was not completely inhibited in the isogenic *pta* mutant (Fig. 10). During the preparation of this manuscript, Rocha *et al.* published a report suggesting a role for *mrpA* (encodes the major pilin of MR/P fimbria) in the autoaggregation of *P. mirabilis* (Rocha *et al*., 2007). In their studies MrpA contributed to the autoaggregation of the pathogen, but inactivation of the gene did not completely abolish the phenotype. We propose that both MR/P fimbria and Pta play a role in autoaggregation in *P. mirabilis*, but their expression in the host may be spatially or temporally regulated. We have also identified that pH is a critical factor in the induction of Pta (Fig. 8, and Table 2), hence, *P. mirabilis* may co-ordinate the expression of Pta under circumstances that are different from that of MrpA.

Autotransporters with bi- or tri-functional phenotypes, such as adhesion, invasion and autoaggregation, are not uncommon; however, the combination of autoaggregation and cytotoxic functions makes Pta unique. ATs that elicit cytopathic effects (e.g. Pet, Sat or VacA) on the host are shown to release their passenger domain into the extracellular milieu. In the case of Pta, the passenger domain remains intact with its translocator domain in the OM but still functions as a cytotoxic protease. ATs that mediate cell–cell aggregation, haemagglutination or adhesion to the host cell have not been shown to elicit cytopathic effects on the host as seen with Pta. Thus *P. mirabilis* Pta illustrates the diverse mechanisms by which ATs can augment the virulence of Gram-negative pathogens.

Pta is a newly recognized virulence factor in *P. mirabilis*. *Proteus* infections can be more serious than their *E. coli* counterparts as they are often complicated by renal stone formation, and are not always responsive to antibiotic therapy (Mobley, 1996a). A repertoire of established virulence factors contributes to these complicated ascending UTIs. A few of these are strongly immunogenic (Li and Mobley, 2002, Coker *et al*., 2000) including flagellin (FlaA), fimbrial adhesin (MrpH) and the urease (UreA) (Li *et al*., 2002). The genome sequence of strain HI4320 predicts six putative ATs in this uropathogen. As for the case of Uropathogenic *E. coli* (UPEC) strain CFT073, the six ATs in *P. mirabilis* can be classified as protease-like, adhesin-like or haemagglutinin-like ATs based on their putative function (Pearson *et al*., 2008). In the absence of an effective type III secretion system in *P. mirabilis* (Pearson and Mobley, 2007), it is expected that ATs play a major role in the virulence of this uropathogen. Of these, we have reported the structure–function relationship of the subtilisin-like protease AT encoded by Orf c2341 and, based on its observed phenotype *in vitro*, we named it Pta, for *P*roteus *t*oxic *a*gglutinin. The functions associated with Pta were also shown to be of significant importance in the persistence of the pathogen in the host (Fig. 11).

Cytopathic effects caused by *P. mirabilis* in infected individuals have been an issue of critical clinical importance. Elegant studies in the early 1990s significantly contributed into identifying the roles of haemolysin (HpmA) and urease in the cytotoxic effects of *P. mirabilis in vitro* using cultured epithelial cells (Swihart and Welch, 1990; Mobley *et al*., 1991; Chippendale *et al*., 1994). Even though the phenotype was shown to be *hpmA* dependent *in vitro*, there was no significant difference in the histology of bladder and kidney of mice infected with either the wild type or the isogenic *hpmA* mutant (Swihart and Welch, 1990). Based on these results the authors predicted a role for other unknown virulence factors that contributed to the observed cytotoxicity of the *hpmA* mutant in the host (Swihart and Welch, 1990).

Table 3. Primers used in this study.

Name	5′–3′ sequence	Restriction site
PTA-For	AGGTACAGA***GGATCC***ATGAACAAAGAAATA	*Bam*HI
PTA-Rev	ATAAGGT***CTCGAG***TTAGAAATTAATTTTCAATAT	*Xho*I
PTA-Rev His	ATAAGGA***CTCGAG***GAAATTAATTTTCAATATTGC	*Xho*I
PTA-Alpha	TAGTT***CTCGAG***AAACTACCACTGATGGTTTT	*Xho*I
PTA-844	TTCCA***CTCGAG***GCACCTAATAACCCA	*Xho*I
PTA-910	GTGTT***CTCGAG***TTTTGGCATCTCTATCTTG	*Xho*I
PTA-1016	AATAAA***CTCGAG***TTATCTAGTTTACCACCTCG	*Xho*I
PTA-1054	TTAGAG***CTCGAG***ATACCGAAAGTGGTTGATTT	*Xho*I
PTA-BADF	AGTTTA***CTCGAG***TCCCTTTCAACATAACAGAAGGTA	*Xho*I
PTA-BADR	ATAAGGT***AAGCTT***TTAGAAATTAATTTTCAATATTGCATTAAT	*Hind*III
PTAS366A	CCAGGTTGGGATACCTTTGCTGGTACTGCAATGGCAGCTCCTCATG	
PTAS366AREV	CATGAGGAGCTGCCATTGCAGTACCAGCAAAGGTATCCCAACCTGG	
PTAH147AFOR	AAAGGGGTGAATGATACCGCTGGCACACATGTCACTGG	
PTAH147AREV	ATCAAAGGGGTGAATGATACCCATGGCACACATGTCACTGGTAC	
PTARTF	TGCGATGTAGGATCAGGATTGCCA	
PTARTR	AAATGCGACACCGCTTGATGTGTG	
RPOARTF	GCAAATCTGGCATTGGCCCTGTTA	
RPOARTR	TAGGGCGCTCATCTTCTTCCGAAT	

We suggest that in earlier *in vivo* studies by Swihart *et al.* (Swihart and Welch, 1990), AT Pta together with other uncharacterized protease-like ATs may have contributed to the background cytotoxicity in mice infected with the *hpmA* strain. In this study we have demonstrated that growth in alkaline and calcium-rich medium conditions that mimic the host during *Proteus* infection is required for expression and activity of Pta. These conditions were instrumental in identifying the role of Pta in the cytotoxicity exhibited by *P. mirabilis*. However, further studies to compare the histopathology of mice infected with wild-type or the *pta hpmA* double mutant will be helpful in determining the precise role of Pta in the pathogenesis of *P. mirabilis* infections.

In conclusion, we identified a novel bi-functional AT protein, Pta, as an important virulence factor in the uropathogen *P. mirabilis*. This study not only opens a new area for further research in the field of *Proteus* but also provides a wide scope for research in the rapidly growing field of AT proteins. ATs have also been tested for use as antigens in subunit or multivalent vaccines against Gram-negative pathogens (Wells *et al.*, 2007). Hence, further investigation into the antigenic properties of Pta may make it a valuable resource in our ongoing efforts to design a multivalent vaccine against *Proteus*.

Experimental procedures

Bacterial strains and plasmids

Bacterial strains and plasmids used in this study are listed in Table 3. Uropathogenic *P. mirabilis* catheter-associated strain HI4320 was used as parent wild-type strain. *E. coli* Top10 was used for DNA manipulations. Plasmid pET21A that contains IPTG-inducible T7 promoter was used for overexpressing the protein in *E. coli* BL21plysS.

Media and reagents

Luria–Bertani broth (LB broth) or agar contained 5 g l^{-1} and 0.5 g l^{-1} NaCl for *E. coli* and *P. mirabilis* respectively. Media were supplemented with ampicillin (100 μg ml^{-1}), kanamycin (25 μg ml^{-1}), chloramphenicol (20 μg ml^{-1}) and tetracycline (15 μg ml^{-1}) as appropriate. Leupeptin, chymostatin, STI, BBI, TLCK, TPCK, DFP, PMSF, the *p*-nitroanilide (–*p*Na) substrates *N*-Suc–Ala–Ala–Pro–Phe–*p*Na, *N*-Suc–Ala–Ala–Pro–Leu–*p*Na, benzoyl–Arg–*p*Na (BA*p*Na), *N*-Suc–Ala–Ala–Pro–Val–*p*Na, *N*-Suc–Ala–Ala–Ala–*p*Na were all purchased from Sigma-Aldrich Chemical Company (St Louis, MO).

In silico *analyses*

The putative amino acid sequence of PMI2341 was analysed by BLAST (http://www.ncbi.nih.gov./blast) to determine its sequence identity and similarity with other known proteins. Sequence alignments and analyses were performed using the bioinformatic program suite available at (http://usexpasy.org). Signal peptide was predicted using SignalP (http://www.cbs.dtu.dk/services/SignalP). Identification of amino acid residues that form the putative catalytic site of the protease and that form the beta domain of the AT was performed using MOTIF search (http://motif.genome.jp/). The topology of the beta domain (OM spanning hydrophobic residues and the connecting hydrophilic loops) in the C-terminus of the protein was predicted using PredictProtein (http://www.predictprotein.org/).

Cloning and overexpression of Pta E. coli *BL21plysS*

The 3.2 kb gene *pta* (PMI2341) was amplified by PCR from the genomic DNA of HI4320 using primers PTA-For and PTA-Rev (lacking the stop codon) carrying BamHI and XhoI sites, respectively, at their 5′ ends. The PCR product was cloned into the compatible restriction sites in the expression vector pET21A to generate plasmid to facilitate the expression of a C-terminal 6X-His-tagged fusion protein.

Table 4. Plasmids and strains used in this study.

Plasmid	Features and application	Reference
pSAP2000B	*pta* cloned into the *Bam*HI–*Xho*I sites in pET21A to express C-terminus 6X-His-tagged Pta	This study
pSAP2010	*pta* with S365A point mutation cloned into the *Bam*HI–*Xho*I sites in pET21A to express C-terminus 6X-His-tagged Pta	This study
pSAP2032	Alpha domain of Pta cloned into the *Bam*HI–*Xho*I sites of pET21A to express C-terminus 6X-His-tagged Pta-α	This study
pSAP2012	*pta* gene segment corresponding to 844 amino acids towards the N-terminus cloned into the *Bam*HI–*Xho*I sites of pET21A	This study
pSAP2013	*pta* gene segment corresponding to 1016 amino acids towards the N-terminus cloned into the *Bam*HI–*Xho*I sites of pET21A	This study
pSAP2015	*pta* gene segment corresponding to 910 amino acids towards the N-terminus cloned into the *Bam*HI–*Xho*I sites of pET21A	This study
pSAP2018	*pta* gene segment corresponding to 1054 amino acids towards the N-terminus cloned into the *Bam*HI–*Xho*I sites of pET21A	This study
pSAP2034	*pta* cloned into the XhoI–HindIII sites of pBAD-Myc-His-A for overexpression in *P. mirabilis* HI4320	This study
pSAP2037	pACD4K (Sigma) carrying retargeted intron with *pta* homologous sequences. The plasmid is used for insertional inactivation of Pta in *P. mirabilis* HI4320 and BA6163	This study
pSAP2038	Alpha domain of Pta with the S366A point mutation cloned into the *Bam*HI–*Xho*I sites of pET21A to express C-terminus 6X-His-tagged Pta-$\alpha_{(S366A)}$	This study
pSAP2039	*pta* with the S366A point mutation cloned into the XhoI–HindIII sites of pBAD-Myc-His-A for overexpression in *P. mirabilis* HI4320	This study
pSAP2040	The alpha domain of Pta with the H147A point mutation cloned into the BamHI–HindIII sites of pET21A to express a C-terminus 6X-His-tagged Pta-$\alpha_{(H147A)}$	This study
pSAP2041	*pta* carrying active-site point mutations S366A and H147A	This study
pSAP2042	pET21A carrying Pta with C-terminal point mutations Y1063A, F1065A and Y1067A	This study
HI4320	*P. mirabilis* catheter-associated wild-type strain. Tetracycline resistant	Clinical isolate
BA6163	*P. mirabilis* urinary tract isolate. Tetracycline resistant	Clinical isolate
ALM2000	Insertional inactivation of Pta using pSAP2037 in HI4320	This study
ALM2001	HI4320 expressing empty pBAD-*Myc*-His-A vector as control	This study
ALM2002	HI4320 expressing pSAP2034	This study
ALM2003	ALM2000 expressing empty pBAD-*Myc*-His-A control	This study
ALM2004	ALM2000 expressing pSAP2034	This study
ALM2005	HI4320 expressing pSAP2039	This study
ALM2006	ALM2000 expressing pSAP2039	This study

Strategene's Quick Change® Site Directed Mutagenesis kit was used to create point mutations at nucleotides corresponding to residue Ser366 and construct an active-site serine mutant of Pta in plasmid pSAP2010. Primers (PtaS366AFor and PtaS366ARev) were designed as directed by the manufacturer, and plasmid pSAP2000B was used as the template DNA. To generate a S366A and H147A, primers (HIS147AFor and HIS147ARev) were used to generate His147 to Ala147 point mutation in pSAP2010 (which carries S366A mutation). The resulting plasmid was designated pSAP2041 (Table 4). Point mutations were confirmed by sequencing the resulting plasmids at the University of Michigan DNA Sequencing Core facility.

To overexpress Pta (or its active-site Ser mutant), plasmid pSAP2000B or pSAP2010 were individually transformed into the overexpression strain *E. coli* BL21plysS. *E. coli* BL21plysS transformed with pET21A alone was used as vector control. Overnight culture of *E. coli* BL21plysS carrying the *pta* clone or the vector control was inoculated to a 1:100 dilution into fresh LB broth supplemented with ampicillin (100 μg ml^{-1}) and chloramphenicol (20 μg ml^{-1}) and cultured at 37°C with constant shaking to an OD_{600} of 0.6. IPTG was added to the culture to a final concentration of 1 mM and the expression was induced for 3 h. Protein expression was confirmed by running whole-cell extracts of *E. coli* expressing *pta*, $pta_{(S366A)}$ or the vector control on 10% SDS-PAGE followed by staining with Commassie Brilliant Blue.

Purification of C-terminus 6X-His-tagged Pta, $Pta_{(S366A)}$ or $Pta_{(S366A/H147A)}$

Escherichia coli BL21plysS carrying the clone of interest was harvested after a 3 h induction with IPTG. Bacteria were lysed using French Pressure Cell (20 000 psi) and the lysate was centrifuged (14 000 *g*, 10 min, 4°C) to separate unbroken cells. Cytoplasmic and membrane protein fractions were separated by ultracentrifugation of the cell-free extract (100 000 *g*, 1 h, 4°C). Inner membrane was selectively solubilized by re-suspending the pellet in 2% Sodum Lauryl Sarkosyl in 10 mM Tris-Cl (pH 7.5) and centrifugation (10 000 *g*, 1 h, 4°C). The pellet containing the OM was solubilized using 1% zwittergen 4-14 (non-ionic detergent) in Buffer A (50 mM $NaPO_4$, 300 mM NaCl, 10 mM imidazole, pH 8.0) and rocked at room temperature for 1 h. The suspension was centrifuged (100 000 *g*, 1 h, 4°C) and the supernatant containing the soluble OM was collected. Zwittergen percentage was brought down to 0.1% by diluting the protein with Buffer A. The highly enriched ~30 kDa OmpA protein (identified by MALDI-TOF/MS) served as a marker to confirm successful enrichment OM protein fraction using this procedure. The OM protein suspension was mixed with slurry of 50% Ni-NTA (Qiagen) and rocked at 4°C for 1 h to facilitate binding of the protein to the Ni-NTA resin. The Ni-NTA and protein slurry was washed with 10 column volumes of Buffer B (50 mM Na phosphate, 300 mM NaCl and 30 mM imidazole, pH 8.0) and

finally eluted with Buffer C (50 mM Na phosphate, 300 mM NaCl and 250 mM imidazole, pH 8.0 containing 0.05% zwittergen). Protein purity was determined by running the fractions on a 10% SDS-PAGE followed by Commassie staining. Pure aliquots were dialysed against 1 l of Buffer A with 0.015% zwittergen at 4°C for 2 days. Protein was electrophoresed on 10% SDS-PAGE and bands were cut out of the gel and identified by MALDI-TOF/MS at the University of Michigan Protein Consortium. Protein was concentrated and quantified using BCA assay (Pierce). To identify both potential signal sequence and the secondary cleavage site in Pta, the purified protein fraction was electrophoresed on a 10% SDS-PAGE, transblotted onto a PVDF membrane and the amino black stained bands were excised for N-terminus sequencing at Emory School of Medicine Research Core Laboratories.

C-terminal truncations of Pta and their cellular localization

The amino acid sequence of Pta was subjected to secondary structure prediction by PredictProtein and the regions of high hydrophobicity with potential for forming antiparallel beta sheets and the connecting hydrophilic loops were determined as described earlier. Nine different regions with the potential of forming antiparallel beta sheets and eight connecting hydrophilic coils were identified. Primers were designed to obtain C-terminus truncations at four of the eight connecting regions (at residues 844, 910, 1016 and 1054) that were approximately at 30-amino-acid intervals (Table 4). These truncated genes were amplified by PCR using the Pta-For and the corresponding 3′ primer (carrying the restriction site for XhoI) and the individual PCR products were cloned into pET21A vector. To generate Pta-1072*, nucleotide sequences corresponding to amino acid residues Tyr1063, Phe1065 and Tyr1067 were altered to the respective alanines using Strategene's Quick Change® Site Directed Mutagenesis kit using plasmid pSAP200B as template. The resulting plasmid was designated pSAP2042. All clones were confirmed by DNA sequencing at the University of Michigan DNA Sequencing Core facility. Vectors carrying various truncations were individually transformed into *E. coli* BL21plysS and were overexpressed as described previously. Cytoplasmic and OM fractions for each truncated protein were enriched using a similar procedure as described above. Protein (10 μg) from each mutant was run on a 10% SDS-PAGE. Truncated Pta was detected by immunoblotting using 1:750 dilution of Anti-Pta antibody and 1:30 000 of Goat Anti-Rabbit IgG-Horse Radish Peroxidase (HRP) conjugate.

Purification of C-terminal 6X-His-tagged Pta-α and its active-site variants

DNA corresponding to the passenger domain of the AT (amino acids 1–730) was amplified using primers PTAFor and Pta730Rev and cloned into expression vector pET21A. Active-site variants (S366A and H147A) were obtained using Strategen's Quick Change® Site Directed Mutagenesis Kit in a similar procedure as described above. The proteins were individually expressed in *E. coli* BL21plysS and were affinity purified from the cytoplasmic protein mixture of *E. coli* BL21plysS using Ni-NTA agarose resin. The same buffers used for Pta-6X-His were used here but without the detergent. The purified protein was electrophoresed on a 12% SDS-PAGE and the bands were excised to confirm the protein identity by MALDI-TOF/MS.

Protease activity

Proteolytic activity was measured using the above mentioned chromogenic substrates in 50 mM $NaPO_4$ buffer, pH 8.5, containing 20 mM $CaCl_2$ and 0.005% Triton X-100. Reactions were performed in white-bottom 96-well plates containing the appropriate amount of protease, a range of substrate concentrations (10–150 μM), and reaction buffer to a final volume of 250 μl. Protease activity was measured as an increase in the OD_{412} due to cleavage of substrate at 37°C. A unit of protease activity was defined as micromoles substrate cleaved per milligram of protein per minute. Where noted, a unit activity was defined as the amount of enzyme that caused an increase in the absorbance by 0.1 per min.

For determination of pH optimum, pure protein was first incubated in carbonate buffers (pKa 2.3 and 6.4) with different pH ranging from 5.5 to 11 and its stability was assessed by running on a 10% SDS-PAGE. The effect of pH on the protease activity to *N*-Suc–Ala–Ala–Pro–Phe–*p*Na was assayed with the above mentioned buffer in the pH range between 5.5 and 11. Reactions were carried out as described above with a standard substrate (100 μM) and enzyme (50 nM) concentrations. Activity was determined by cleavage of the substrate and was monitored at OD_{412}.

To determine the effect of inhibitors, the enzyme (50 nM) was allowed to complex with an inhibitor (10 mM) for 30 min in the above mentioned buffer and the residual protease activity was measured using 100 μM *N*-Suc–Ala–Ala–Pro–Phe–*p*Na as described above.

Interaction of bacterial cells with epithelial monolayer

Interaction of Pta with epithelial cell monolayer was assessed using whole cells of *E. coli* BL21plysS expressing Pta or its active-site serine variant. Briefly, human kidney epithelial cells (HEK293), human bladder epithelial cells (UMUC3), mouse kidney epithelial (MMK.5) or Hamster kidney epithelial (BHK21) were cultured as monolayers in 24-well tissue culture-treated plate containing DMEM supplemented with 10% FBS, 10 μg ml^{-1} penicillin/streptomycin and 10 μg ml^{-1} glutamine. For microscopic examination, monolayers were cultured on poly L-lysine-treated 12 mm coverslips in 24-well plates. Prior to inoculation with bacterial cells, the medium was changed to pre-warmed DMEM with 10% glutamine. To examine the interaction of *E. coli* BL21plysS (5×10^7 cells) expressing either the vector alone, Pta or $Pta_{(S365A)}$ were overlaid onto tissue culture cells. The plate was centrifuged at 500 *g* for 5 min and incubated at 37°C for 45 min. For the quantitative cell adhesion assay wells were washed (5×) with PBS, pre-warmed to 37°C, to remove any unbound bacterial cells. The wells were then treated with 0.25% trypsin-EDTA to remove the bound monolayer and various dilutions were plated on LB agar plates. For microscopic examination, the monolayer was fixed with 4% paraformaldehyde for 10 min

after initial washes. Fixative was aspirated and the wells were washed (3×) with PBS and stained with Giemsa (1:30 in 10% methanol) for 15 min followed by destaining with 10% methanol. Coverslips were dried and mounted onto the glass slides. Similar procedure was followed to study the interaction of various strains of *P. mirabilis* with different epithelial cell lines. Slides were examined using Olympus BX60 immunofluorescence microscope and images were taken using Olympus DP70 camera. For quantitative estimation, epithelial cells were grown in poly L-lysine-treated 96-well plates and infected with *E. coli* cells expressing various versions of Pta. After incubation for 1 h at 37°C, the supernatant was collected and LDH release was estimated as described below.

Interaction of pure protease with the host cells

To determine the interaction of purified Pta, Pta-α or their active-site variants with the host, bladder or kidney epithelia were cultured in tissue culture-treated multichamber glass slides containing DMEM supplemented with 10% FBS + 5 μg ml^{-1} streptomycin/penicillin and 10 μg ml^{-1} glutamine. Medium was changed to pre-warmed DMEM + 10% glutamine and the cells were treated with known amounts of Pta or the buffer control and incubated at 37°C. At various time intervals, chambers were washed (5×) with PBS, fixed and stained with Giemsa as described above. For immunofluorescent detection of cell morphology, cells were fixed, permeabilized by treating with 0.1% Triton-X in PBS for 10 min. The slides were then washed (3×) with pre-warmed PBS and blocked with 2% BSA for 1 h at 30°C followed by staining with FITC-phalloidin and DAPI (both in PBS with 1% BSA) under dark for 30 min at room temperature (Product No. F432 and D3571, Invitrogen, CA, USA). Slides were washed (5×) with PBS, air-dried and mounted using Prolong Gold Anti-Fade® (Invitrogen; Product No. P36930) covered and incubated at 4°C overnight. Slides were examined using Olympus BX60 immunofluorescence microscope and the images were recorded with an Olympus DP70 camera.

Quantitative estimation of cytotoxicity by lactate dehydrogenase release

Extent of host cell lysis was estimated indirectly by measuring the release of intracellular lactate dehydrogenase from the nucleated cells using Cytox® Membrane Permeability Assay from Promega, Madison, USA (Product No. G7890) as described elsewhere (Kehl-Fie and St Geme, 2007). Briefly, epithelial cells were cultured in poly L-lysine-treated 96-well plates in the above described medium. Medium was changed to DMEM + 10% glutamine prior to infection with a known concentration of either purified wild-type Pta, Pta-α or their active-site variants and incubated at 37°C. Plates were removed at various time points and the substrate reagent was added to all wells and incubated by brief shaking at room temperature for 20 min. Stop solution was added to the wells and the fluorescence was measured at 560–590 nm on Synergy™ HT Multi-Detection Microplate reader from Bio Tek. Treatment with PBS containing 0.015% Zwitterngen and with 2.5% Triton X-100 was used as controls. Cytotoxicity of the protein was expressed as a per cent of maximum cell lysis obtained by Triton X-100 treatment after normalizing the values obtained from treatment with buffer only control.

Construction of a pta *mutant and complementation* in trans

Targetron® (Sigma) was used for insertional inactivation of *pta* in HI4320 (Table 4). The procedure was modified as described by Pearson and Mobley (2007). The mutant *pta*Ω*aph*A3 was confirmed PCR and sequencing and also using polyclonal Anti-Pta antibody.

For complementation, wild-type copy of *pta* was cloned into the overexpression vector pBAD Myc-His. The active-site Ser366Ala variant was obtained by a similar procedure as described earlier but by using pBAD-*pta* as the template. The vector carrying either the wild type or the site-directed mutant was transformed into *pta*Ω*aph*A3 to complement *in trans*. Percentage of arabinose was titrated to control the level of Pta expression in the mutant to that of the expression in the wild-type strain. We found that induction with 2% arabinose for 2 h produced enough protein to match with the expression levels to that of the wild-type strain. The percentage of arabinose was increased to 5% to overexpress the *pta* either in the wild type or the isogenic *pta* mutant, and the amount of Pta in the latter was found to be at least threefold higher than in the 2% induced cells. Complementation was confirmed by immunostaining the OM fractions with polyclonal anti-Pta antibody (1:1000) followed by staining with Goat Anti-Rabbit IgG-HRP conjugate (1:50 000). Protein bands were visualized by chemiluminescent detection using ECL Western Blotting Detection Substrate (Product No. RPN2106) from Pierce, Rockland, IL, USA.

Effect of growth conditions in the expression of pta *in* P. mirabilis *HI4320*

Proteus mirabilis wild-type strain HI4320 was grown under different conditions of temperature (25°C, 37°C and 42°C), pH (5.0, 7.0 and 9.0), salt concentration (0.5 M NaCl), iron stress (0.5 mM $FeSO_4$ or 15 μM desferral), metal ion supplementation (0–5 mM $MgCl_2$ or 20 mM $CaCl_2$; independently at pH 7.0 and pH 9.0). The OM fraction was extracted independently from each of the above conditions and the presence of Pta was determined by immunostaining with Anti-Pta polyclonal antisera. Intensity of Pta-specific bands was quantified using ImageJ software from http://www.nih.gov and fold increases or decreases in protein expression in each case was compared with that expressed in exponential-phase bacteria cultured at 37°C in LB pH 7.0. Alternatively, quantitative RT-PCR was performed to measure expression of *pta*, and *P. mirabilis* strains were cultured to mid-exponential phase (OD_{600} = 0.8) under each of the above said conditions. RNAprotect (2 ml) (Qiagen) was added to 1 ml of culture, and RNA was isolated using the RNeasy kit (Qiagen) according to the manufacturer's instructions. DNA was digested using TURBO DNA-*free* DNase (Ambion). RNA was used as the template for cDNA synthesis using the Superscript First-Strand Synthesis System (Invitrogen) according to the manufacturer's protocol. *rpoA* (DNA-dependent RNA polymerase Alpha) was used as the normalizer and RNA isolated from

P. mirabilis HI4320 cultured at 37°C in LB pH 7.0 was used as the calibrator. Fold change in expression of *pta* was expressed relative to the calibrator.

Interaction of P. mirabilis *with eukaryotic hosts*

Confluent epithelial cell monolayers were obtained as described earlier. Wild type, mutant or either strains overexpressing *pta* on plasmid were cultured in LB broth supplemented with 4% glycerol and 20 mM $CaCl_2$. The pH was adjusted to 8.5 using potassium phosphate. Where appropriate, bacteria were cultured until OD_{600} equalled 0.6 and induced with 5% arabinose for 3 h. Cells were washed with PBS (3×) and re-suspended in phosphate buffer (pH 8.5) and overlaid onto confluent bladder or kidney epithelial cells to assess Pta-mediated interaction. LDH release from the eukaryotic host was estimated as described above.

Autoagglutination assay

To quantitatively estimate autoagglutination by *P. mirabilis*, various strains were cultured, induced and processed as described above. Cells were finally re-suspended in 10 ml of phosphate buffer (pH 8.5) to a cell density of 450–480 Klett units. Cell density (Klett units) was measured at different time points using Klett-Summerson Photoelectric Colorimeter (Klett MFG, NY, USA). The drop in Klett unit reading from the initial cell density of 450–480 units together with the formation of clumping in the bottom of the tube reflects the degree of autoagglutination.

Mouse model of ascending UTI

The CBA/J mouse model of ascending UTI has been described previously (Li *et al*., 1999). Briefly, 6-week-old female CBA/J mice were inoculated transurethrally with a 50 µl suspension of 5×10^7 cfu of *P. mirabilis* HI4320 wild type and the *pta*Ω*aph*A3 mutant (1:1). At 7 days post infection, urine, and the tissue homogenates of bladders, kidneys, and spleen of the mice were examined for the presence of *P. mirabilis* by plating on LB and LB + Kan (25 µg ml^{-1}) using a spiral plater (Autoplate 4000, Spiral Biotech). Colony counts were enumerated using a QCount (Spiral Biotech) and expressed as cfu per gram of tissue or cfu per millilitre of urine. Statistical significance of the data was determined using the Wilcoxon matched pairs test.

Acknowledgements

We are thankful to Sara N. Smith for her substantial assistance in mouse colonization assays. Thanks are also due to Amy N. Simms, Stēphane L. Benoit and Suleyman Felek for critical reading of this manuscript and Smitha Thatha for proof reading and formatting of figures. The project was funded by public health service Grant AI-059722 from the National Institutes of Health to H.L.T.M. MALDI-TOF MS/MS analysis was provided by the Michigan Proteome Consortium (http://www.proteomeconsortium.org) which is supported in part by funds from the Michigan Life Sciences Corridor.

References

Backert, S., and Meyer, T.F. (2006) Type IV secretion systems and their effectors in bacterial pathogenesis. *Curr Opin Microbiol* **9:** 207–217.

Cainelli Gebara, V.C., Risoleo, L., Lopes, A.P., Ferreira, V.R., Quintilio, W., Lepine, F., *et al.* (2007) Adjuvant and immunogenic activities of the 73 kDa N-terminal alpha-domain of BrkA autotransporter and Cpn60/60 kDa chaperonin of *Bordetella pertussis*. *Vaccine* **25:** 621–629.

Chippendale, G.R., Warren, J.W., Trifillis, A.L., and Mobley, H.L. (1994) Internalization of *Proteus mirabilis* by human renal epithelial cells. *Infect Immun* **62:** 3115–3121.

Cianciotto, N.P. (2005) Type II secretion: a protein secretion system for all seasons. *Trends Microbiol* **13:** 581–588.

Coker, C., Poore, C.A., Li, X., and Mobley, H.L. (2000) Pathogenesis of *Proteus mirabilis* urinary tract infection. *Microbes Infect* **2:** 1497–1505.

Cotter, S.E., Surana, N.K., and St Geme, J.W., 3rd (2005) Trimeric autotransporters: a distinct subfamily of autotransporter proteins. *Trends Microbiol* **13:** 199–205.

Cotter, S.E., Surana, N.K., Grass, S., and St Geme, J.W., 3rd (2006) Trimeric autotransporters require trimerization of the passenger domain for stability and adhesive activity. *J Bacteriol* **188:** 5400–5407.

Girard, V., and Mourez, M. (2006) Adhesion mediated by autotransporters of Gram-negative bacteria: structural and functional features. *Res Microbiol* **157:** 407–416.

Guyer, D.M., Radulovic, S., Jones, F.E., and Mobley, H.L. (2002) Sat, the secreted autotransporter toxin of uropathogenic *Escherichia coli*, is a vacuolating cytotoxin for bladder and kidney epithelial cells. *Infect Immun* **70:** 4539–4546.

Harris, P.R., Cover, T.L., Crowe, D.R., Orenstein, J.M., Graham, M.F., Blaser, M.J., and Smith, P.D. (1996) *Helicobacter pylori* cytotoxin induces vacuolation of primary human mucosal epithelial cells. *Infect Immun* **64:** 4867–4871.

Henderson, I.R., and Nataro, J.P. (2001) Virulence functions of autotransporter proteins. *Infect Immun* **69:** 1231–1243.

Henderson, I.R., Navarro-Garcia, F., and Nataro, J.P. (1998) The great escape: structure and function of the autotransporter proteins. *Trends Microbiol* **6:** 370–378.

Henderson, I.R., Czeczulin, J., Eslava, C., Noriega, F., and Nataro, J.P. (1999) Characterization of pic, a secreted protease of *Shigella flexneri* and enteroaggregative *Escherichia coli*. *Infect Immun* **67:** 5587–5596.

Henderson, I.R., Navarro-Garcia, F., Desvaux, M., Fernandez, R.C., and Ala'Aldeen, D. (2004) Type V protein secretion pathway: the autotransporter story. *Microbiol Mol Biol Rev* **68:** 692–744.

Hutton, J.C. (1990) Subtilisin-like proteinases involved in the activation of proproteins of the eukaryotic secretory pathway. *Curr Opin Cell Biol* **2:** 1131–1142.

Johnson, D.E., Russell, R.G., Lockatell, C.V., Zulty, J.C., Warren, J.W., and Mobley, H.L. (1993) Contribution of *Proteus mirabilis* urease to persistence, urolithiasis, and acute pyelonephritis in a mouse model of ascending urinary tract infection. *Infect Immun* **61:** 2748–2754.

Kehl-Fie, T.E., and St Geme, J.W., 3rd (2007) Identification

and characterization of an RTX toxin in the emerging pathogen *Kingella kingae*. *J Bacteriol* **189:** 430–436.
Klemm, P., Vejborg, R.M., and Sherlock, O. (2006) Self-associating autotransporters, SAATs: functional and structural similarities. *Int J Med Microbiol* **296:** 187–195.
Kluskens, L.D., Voorhorst, W.G., Siezen, R.J., Schwerdtfeger, R.M., Antranikian, G., van der Oost, J., and de Vos, W.M. (2002) Molecular characterization of fervidolysin, a subtilisin-like serine protease from the thermophilic bacterium *Fervidobacterium pennivorans*. *Extremophiles* **6:** 185–194.
Li, X., and Mobley, H.L. (2002) Vaccines for *Proteus mirabilis* in urinary tract infection. *Int J Antimicrob Agents* **19:** 461–465.
Li, X., Johnson, D.E., and Mobley, H.L. (1999) Requirement of MrpH for mannose-resistant *Proteus*-like fimbria-mediated hemagglutination by *Proteus mirabilis*. *Infect Immun* **67:** 2822–2833.
Liu, D.F., Mason, K.W., Mastri, M., Pazirandeh, M., Cutter, D., Fink, D.L., *et al.* (2004) The C-terminal fragment of the internal 110-kilodalton passenger domain of the Hap protein of nontypeable *Haemophilus influenzae* is a potential vaccine candidate. *Infect Immun* **72:** 6961–6968.
Mobley, H.L. (1996a) *Urinary Tract Infections: Molecular Pathogenesis and Clinical Management.* Washington, DC: American Society for Microbiology Press, pp. 245–270.
Mobley, H.L. (1996b) Virulence of *Proteus mirabilis*. In *Urinary Tract Infections: Molecular Pathogenesis and Clinical Management*. Mobley, H.L., and Warren, J.W. (eds). Washington, DC: American Society for Microbiology Press, pp. 245–269.
Mobley, H.L., and Warren, J.W. (1987) Urease-positive bacteriuria and obstruction of long-term urinary catheters. *J Clin Microbiol* **25:** 2216–2217.
Mobley, H.L., Chippendale, G.R., Swihart, K.G., and Welch, R.A. (1991) Cytotoxicity of the HpmA hemolysin and urease of *Proteus mirabilis* and *Proteus vulgaris* against cultured human renal proximal tubular epithelial cells. *Infect Immun* **59:** 2036–2042.
Mota, L.J., and Cornelis, G.R. (2005) The bacterial injection kit: type III secretion systems. *Ann Med* **37:** 234–249.
Navarro-Garcia, F., Sears, C., Eslava, C., Cravioto, A., and Nataro, J.P. (1999) Cytoskeletal effects induced by pet, the serine protease enterotoxin of enteroaggregative *Escherichia coli*. *Infect Immun* **67:** 2184–2192.
Navarro-Garcia, F., Canizalez-Roman, A., Sui, B.Q., Nataro, J.P., and Azamar, Y. (2004) The serine protease motif of EspC from enteropathogenic *Escherichia coli* produces epithelial damage by a mechanism different from that of Pet toxin from enteroaggregative *E. coli*. *Infect Immun* **72:** 3609–3621.
Navarro-Garcia, F., Canizalez-Roman, A., Burlingame, K.E., Teter, K., and Vidal, J.E. (2007) Pet, a non-AB toxin, is transported and translocated into epithelial cells by a retrograde trafficking pathway. *Infect Immun* **75:** 2101–2109.
Paton, A.W., Srimanote, P., Talbot, U.M., Wang, H., and Paton, J.C. (2004) A new family of potent AB(5) cytotoxins produced by Shiga toxigenic *Escherichia coli*. *J Exp Med* **200:** 35–46.
Paton, A.W., Beddoe, T., Thorpe, C.M., Whisstock, J.C., Wilce, M.C., Rossjohn, J., *et al.* (2006) AB5 subtilase cytotoxin inactivates the endoplasmic reticulum chaperone BiP. *Nature* **443:** 548–552.
Pearson, M.M., and Mobley, H.L. (2007) The type III secretion system of *Proteus mirabilis* HI4320 does not contribute to virulence in the mouse model of ascending urinary tract infection. *J Med Microbiol* **56:** 1277–1283.
Pearson, M.M., Sebaihia, M., Churcher, C., Quail, M.A., Seshasayee, A.S., Abdellah, Z., *et al.* (2008) The complete genome sequence of uropathogenic *Proteus mirabilis*, a master of both adherence and motility. *J Bacteriol* (in press).
Rocha, S.P., Elias, W.P., Cianciarullo, A.M., Menezes, M.A., Nara, J.M., Piazza, R.M., *et al.* (2007) Aggregative adherence of uropathogenic *Proteus mirabilis* to cultured epithelial cells. *FEMS Immunol Med Microbiol* **51:** 319–326.
Salama, N.R., Otto, G., Tompkins, L., and Falkow, S. (2001) Vacuolating cytotoxin of *Helicobacter pylori* plays a role during colonization in a mouse model of infection. *Infect Immun* **69:** 730–736.
Seizen, R.J. (1996) Subtilases: subtilisin-like serine proteases. *Adv Exp Med Biol* **379:** 75–93.
Stathopoulos, C., Hendrixson, D.R., Thanassi, D.G., Hultgren, S.J., St Geme, J.W., 3rd, and Curtiss, R., 3rd (2000) Secretion of virulence determinants by the general secretory pathway in gram-negative pathogens: an evolving story. *Microbes Infect* **2:** 1061–1072.
Steiner, D.F. (1998) The proprotein convertases. *Curr Opin Chem Biol* **2:** 31–39.
Stickler, D., Ganderton, L., King, J., Nettleton, J., and Winters, C. (1993) *Proteus mirabilis* biofilms and the encrustation of urethral catheters. *Urol Res* **21:** 407–411.
Swihart, K.G. and Welch, R.A. (1990) Cytotoxic activity of the *Proteus* hemolysin HpmA. *Infect Immun* **58:** 1861–1869.
Tukel, C., Akcelik, M., de Jong, M.F., Simseko, O., Tsolis, R.M., and Baumler, A.J. (2007) MarT activates expression of the MisL autotransporter protein in *Salmonela enterica* serotype Typhimurium. *J Bact* **189:** 3922–3926.
Warren, J.W., Tenney, J.H., Hoopes, J.M., Muncie, H.L., and Anthony, W.C. (1982) A prospective microbiologic study of bacteriuria in patients with chronic indwelling urethral catheters. *J Infect Dis* **146:** 719–723.
Warren, J.W., Damron, D., Tenney, J.H., Hoopes, J.M., Deforge B., and Muncie, H.L., Jr (1987) Fever, bacteremia, and death as complications of bacteriuria, in women with long-term urethral catheters. *J Infect Dis* **155:** 1151–1158.
Wells, T., Tree, J.J., Ulett, G.L., and Schembi, M.A. (2007) Autotransporter proteins: novel targets at the bacterial cell surface. *FEMS Microbiol Lett* **274:** 163–172.

